Structural Determination and Biochemical Analysis of Cadherin-23 Repeats Essential to Hearing

An Undergraduate Research Thesis

Presented in partial fulfillment of the requirements for graduation
with research distinction in Biochemistry in the undergraduate
colleges of The Ohio State University

by

Domenic J. Termine

The Ohio State University
April 2016

Project Advisor: Professor Marcos Sotomayor, Department of Chemistry and Biochemistry
Departmental Representative: Professor Jane Jackman

Table of Contents

Statement of Research

The research presented was conducted under the guidance of Dr. Marcos Sotomayor of The Ohio State University, Department of Chemistry and Biochemistry. I joined *The Sotomayor Research Group* during the Spring of 2014 as a second year biochemistry/pre-medicine student and this thesis is a product of over two years of work, a total of five semesters, and the summer of 2015. I would like to thank Dr. Ottesen, Dr. Gopalan, Dr. Jackman and all other faculty members who generously give their time to help students like myself join research labs through Biochemistry 2900H/2998H. In addition, none of this would be possible without the generous support and funding from Dr. Sotomayor and various affiliates of The Ohio State University.

In 2014, I received The William Marshall MacNevin Memorial Fund Scholarship (Department of Chemistry and Biochemistry) and presented my first semester of work at the Biochemistry Undergraduate Research Forum. In 2015, I received The Bertram Thomas Memorial Fund Scholarship (Department of Chemistry and Biochemistry), an Undergraduate Research Scholarship (College of Arts and Sciences), a Mayers Summer Research Scholarship (Division of Natural and Mathematical Sciences, College of Arts and Sciences), and I presented at the Denman Undergraduate Research Forum. In 2016, I received an Academic Enrichment Grant (Undergraduate Student Government) to attend the Biophysical Society 60th Annual Meeting. I am grateful for the experiences and financial support I have received from research with The Sotomayor Research Group.

Acknowledgements

Dr. Sotomayor was instrumental in all of my accomplishments over the past two years; the design and performance of experiments, the multiple scholarships, production of this thesis, and my acceptance into the University of Cincinnati, College of Medicine. He is a wonderful mentor and despite being the busiest person I know, always makes time to answer any and all questions I may have. Postdocs Dr. Yoshie Narui and Dr. Raul Araya-Secchi are a tremendous support in the lab and I thank them for their expertise, despite how repetitive and concerning my questions may be. Pedro de la Torre Marquez, makes research even more enjoyable with his common phrase, "My friend, what happened", and endless provisions of quality espresso. Even though I feel like most of the graduate students use me as a source of entertainment, I have sincerely enjoyed working with and learning from all of them. Deepanshu Choudhary, spirit animal of the honey badger itself, was helpful in collecting Differential Scanning Fluorimetry data. Avinash Jaiganesh was generous enough to assist with the trypsin assay and has offered a great deal of time fishing and shooting crystals for me. Without the efforts of Adrienne Thornburg, our meetings would be devoid of food and the lab would lose a great deal of personality. Michelle Gray has offered her creative design and Photoshop expertise to make my posters and presentations as beautiful and informative as possible. Sharon Cooper, the magical crystal grower herself, taught me about X-ray crystallography and in which files I could find the necessary parameters for my diffraction set. Last but not least, I would like to thank all of my fellow undergrads for their friendship and never judging me for my singing voice. My family does not understand nor probably care about what I do in the lab, yet they will listen intently and get excited when I eagerly show them pictures of my crystals. Every success, experience, and accomplishment I am blessed with stems from their unconditional love and support.

Thank you

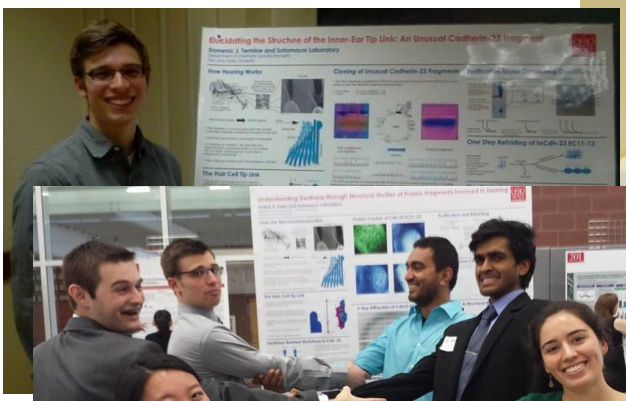

Biophysical Society

LOS ANGELES, CALIFORNIA • FEBRUARY 27 – MARCH 2, 2016
LOS ANGELES CONVENTION CENTER • LA LIVE

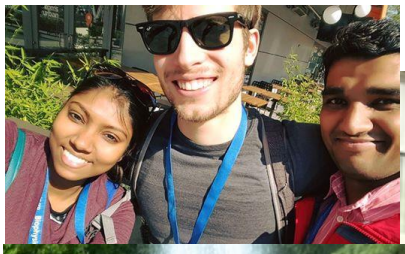

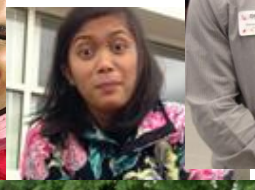

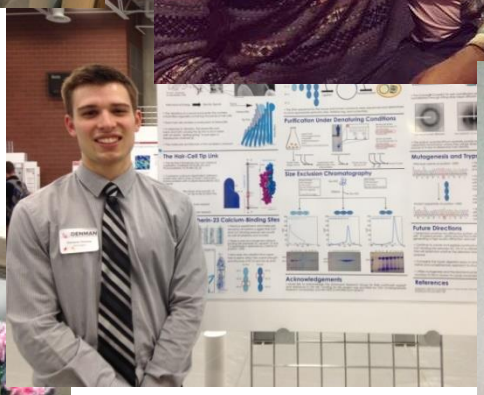

Abstract

Tip links, core components of vertebrate hearing, are thought to directly pull on mechanotransduction channels to transform sound into electrical signals. Cadherin-23 (CDH23) and protocadherin-15 (PCDH15), the two proteins that form the tip link, belong to the cadherin superfamily of calcium (Ca^{2+})-dependent adhesion molecules that feature extracellular cadherin (EC) repeats. These EC repeats are ~100 residues long and are similar, but not identical to each other in terms of fold and sequence. CDH23 features twenty-seven EC repeats and PCDH15 eleven, with calcium-binding sites located at the linkers between them. With all experimental evidence suggesting that Ca^{2+} and highly conserved Ca^{2+}-binding residues are crucial for the elasticity and function of the tip-link, my project focuses on a single Ca^{2+}-binding site between EC12 and EC13 of CDH23 and its unidentified, physiological role in hearing. This site is characterized by a non-canonical sequence SXD (S: serine; X: any residue; D: aspartate) where a serine replaces the first aspartate in what should be the canonical sequence DXD.

Interestingly, a single missense mutation to this unique site, D1341N (SXN), results in non-syndromic deafness. Alternative, but complementary experimentation was employed to characterize and compare wild-type (SXD) and mutant (DXD, SXN) CDH23 fragments. Here, I will present the findings of size-exclusion chromatography experiments, calcium-binding assays, protein crystallization efforts, X-ray diffraction data collection, and a preliminary structure for $EC1+2^{D1355S}$. My goal is to understand why mother nature altered a conserved Ca^{2+}-binding residue in only one out of twenty seven instances and its direct implications on the rigidity and molecular strength of the tip-link. In addition, exploring how D1318N affects vertebrate hearing will allow us to shape scientific study and progress in the direction of eliminating some forms of inherited deafness.

Chapter I: Introduction

Our interaction with the world and the people we share our experiences with is enriched with the gift of hearing – from the inherent peacefulness of wind chimes on a sunny day to the deafening exclamations of O-H-I-O on Saturday afternoons and from the high-pitched squeal of nails on a chalkboard to the low frequency thud of a bass drum. Hearing may have only recently become this specialized by selection in different species, but it is argued that the basis of the vertebrate auditory system arose very early in the evolution of vertebrates. The morphology of the hair cell, the transducing element in all vertebrate ears, can be traced back to our most primitive ancestors, the agnathans and hagfish, some 430 million years ago[1,2].

In its most fundamental form, our two ears must capture mechanical energy, relay it to the receptor organ, and transform this mechanical input to an electrical output that the brain can interpret. The most valuable asset to our hearing system is housed in the inner ear where thousands of hair cells have the capacity to distinguish among an extraordinary frequency range while providing information on both the tones present and their respective amplitudes[3]. However, our hearing system is susceptible to three forms of hearing loss: sensorineural, conductive, or mixed hearing loss[4].

Sensorineural hearing loss comprises any disruption to the cochlea or to the nerve conducting the electrical impulse which could result from illness, loud noises, hereditary or genetic mutations. Equally disruptive but different in form, conductive hearing loss results form an interference in conduction efficiency through the outer or middle ear which involves perforated eardrums, presence of foreign bodies in the canal, or malformations. Conductive hearing loss is often corrected medically or surgically while sensorineural hearing loss is almost always permanent[5].

With 5% of the world's population, some 360 million people, and approximately one-third of all people over 65 years of age suffering from a spectrum of hearing loss, one must ask when and how this debilitating disorder will be counteracted[6]. With the advent of the hearing aid and continual advancement of the cochlear implant, progress is being made to adapt to hearing loss, but not to restore it to its full potential. Unlike amphibians and birds that can induce supporting cells to form new hair cells or zebrafish who have some hair cell populations that are regenerated continually by the activity of stem cells, the 16,000 or so hair cells we are born with cannot be replaced via cell division[3]. Despite extensive research, there is still much to learn about our complex auditory system and new therapies that could someday eliminate forms of deafness will result from this knowledge.

Structure ultimately determines function and The Sotomayor Research Group is working diligently to elucidate the molecular architecture of the tip link, a fine filament consisting of two proteins at the heart of our auditory system. My project focuses on one of these proteins known as cadherin-23, an unusual calcium (Ca^{2+})-binding site within it, and its implications for the rigidity and molecular strength of the tip link as a whole. To understand the importance and role of the tip link, I will begin by introducing the anatomical structure and molecular function of our hearing apparatus from the organ level down to its chemical composition.

1.1 The Architecture of the Outer and Middle Ear

The ear can be anatomically divided into three functional parts: the external, middle, and inner ear (Fig. 1.a). Although the cochlea, our receptor organ, is housed in the inner ear, it cannot function efficiently if the necessary stimulus does not reach that location. Each section of the ear provides an indispensable element to the overall goal of transforming a mechanical stimulus into an electrical signal that the brain can interpret.

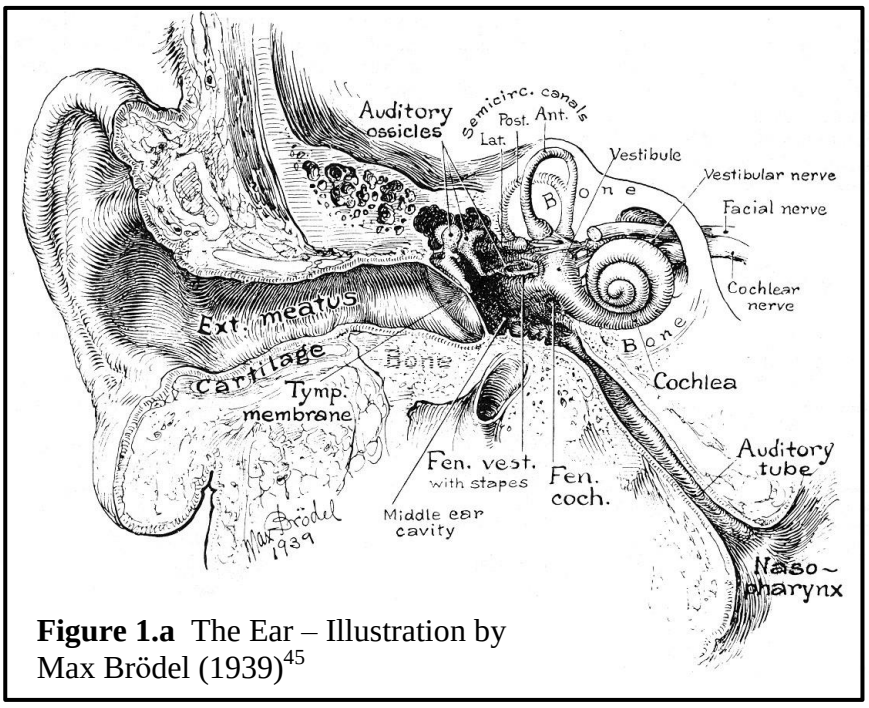

Figure 1.a The Ear – Illustration by Max Brödel (1939)[45]

The outer ear is our tool for efficiently channeling this mechanical energy in the form of sound waves into the external auditory meatus, or ear canal. Observing the unique shape of various ridges and folds of the external ear, it would be unjustified if this comical looking structure did not have a function. The visible portion called the auricle not only allows for the channeling of mechanical energy, but it also serves the purpose of localizing sound in space by reflecting and absorbing certain frequency components of the sound wave[7]. The need to localize sound came about by selective pressure in the evolution of mammalian hearing; it enables us to

utilize our other senses, to direct our eyes, and to make the decision to approach or avoid another animal in our immediate environment[8]. Deep to the auricle, the tympanic membrane, or ear drum, separates the outer ear from the middle ear.

The middle ear is comprised of an air-filled pouch that has a primary role in sound amplification, but also a critical role in pressure equilibration between the middle ear and the pharynx via the Eustachian tube. Here, the airborne sound waves interact with a lever system comprised of three tiny bones called ossicles to efficiently transmit energy from air into liquid, the media inside our inner ear. This chain of connected bones stretches from the tympanic membrane to the oval window in the order of the malleus, incus, and stapes. The mechanism for amplification is analogous to a hydraulic car jack[9]. The surface ratio of eardrum to oval window is 20:1 which allows for efficient transfer of energy to the inner ear. Without this system functioning as an impedance adapter, 98% of energy would be reflected[10].

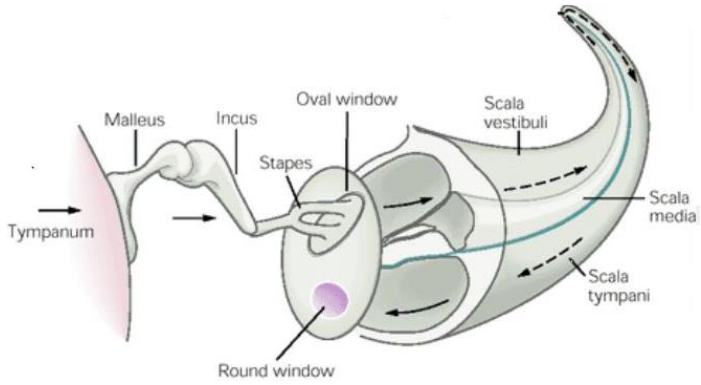

Figure 1.b The wave of force from the ear drum, through the ossicles, and into the fluid of the inner ear. Adapted from [3]

1.2 The Inner Ear and Mechanotransduction

The cochlea of the inner ear functions as the energy converter in this system. At 9 mm across or about the size of a chickpea, this coiled structure of progressively diminishing diameter is wound like a snail's shell. From the base to the topmost portion, the cochlea consists of the scala tympani, the basilar membrane, the scala media, the tectorial membrane, and the scala

vestibule respectively. A ridge of epithelium known as the organ of Corti, extending along the 33 mm basilar membrane, contains 16,000 hair cells and innervation from approximately 30,000 afferent fibers carrying information on the 8th cranial nerve, vestibulocochlear[3].

Residing in this compartment, hair cells and their respective auditory nerve fibers are tonotopically organized; meaning that at any position along the basilar membrane, those hair cells will be more sensitive to a certain frequency. It is known that high frequency sounds stimulate the base of the cochlea, whereas low frequency sounds stimulate the apex[11]. It turns out that both birds and mammals evolved to form specialized inner and outer hair cells around the Triassic-Jurassic periods[12]. Whereas the flask shaped inner hair cells (IHCs) form a single row of approximately 3,500 "transducing" cells, the cylindrical outer hair cells (OHCs) form three rows of approximately 12,000 "amplifier" cells[7,12]. Morphologically, OHCs have the unique property of electromotility in which prestin, a motor protein, drives cellular length changes at different audio frequencies[13].

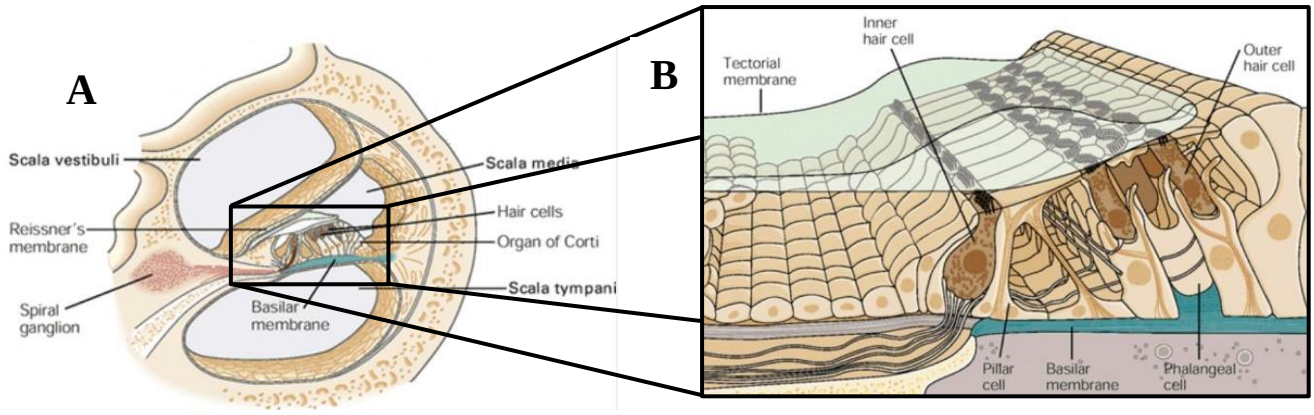

Figure 1.c Inside the Organ of Corti **A)** An illustration of the structural divisions of the inner ear and a zoomed out perspective of the organ of Corti that houses both inner and outer hair cells **B)** A cartoon depiction of the organization of our hair cells. You can see one row of inner hair cells and three rows of outer hair cells above the basilar membrane and below the tectorial membrane. Both of these images are adapted from [3]

On the apical end of each IHC and OHC, we find a sensory "hair" bundle (Fig. 1.d A&B) that serves as the actual organelle of mechanotransduction by responding to fluid movement in the scala media, a liquid known as endolymph that is rich in potassium[14]. This bundle has an eccentrically placed kinocilium, or true cilium, that emerges during the development of the differentiating hair cell and many shorter actin-filled structures called stereocilia. The direction of kinocilium migration predicts the orientation of the mature hair bundle and it regresses postnatally so it is proposed to have only a developmental role. Universal among species, the stereocilia display a monotonic gradient in length along one axis and a tapering at their base where they meet the surface of the hair cell[15] (Fig. 1.d C). These properties serve our hearing apparatus well as a thin, filamentous fiber known as the tip link connects each stereocilia to its neighbor in a staircase design of increasing height (Fig. 1.d D).

Physiologically, our sense of hearing arises from this chain of structures working in parallel. First, vibrations enter the cochlea and forcefully cause the stereocilia to rock back and forth. The stereocilia are arranged in a narrow cleft called the subtectorial space formed by the presence of the stiff tectorial membrane. Here, the OHCs are attached to the tectorial membrane and the IHCs are either free standing or loosely attached[16]. Second, displacement towards the tallest stereocilia causes a shearing action on the tip link which in turn pulls open an ion channel. Finally, the influx of potassium through this open ion channel depolarizes the cell, opens voltage-dependent calcium channels, and releases a neurotransmitter at the basal end of the hair cell creating an action potential in the dendrites of the vestibulocochlear nerve[11] (Fig. 1.d A). At the core of this process are tip links made of cadherin-23 (CDH23) and protocadherin-15 (PCDH15), two enormous cadherins essential for hearing.

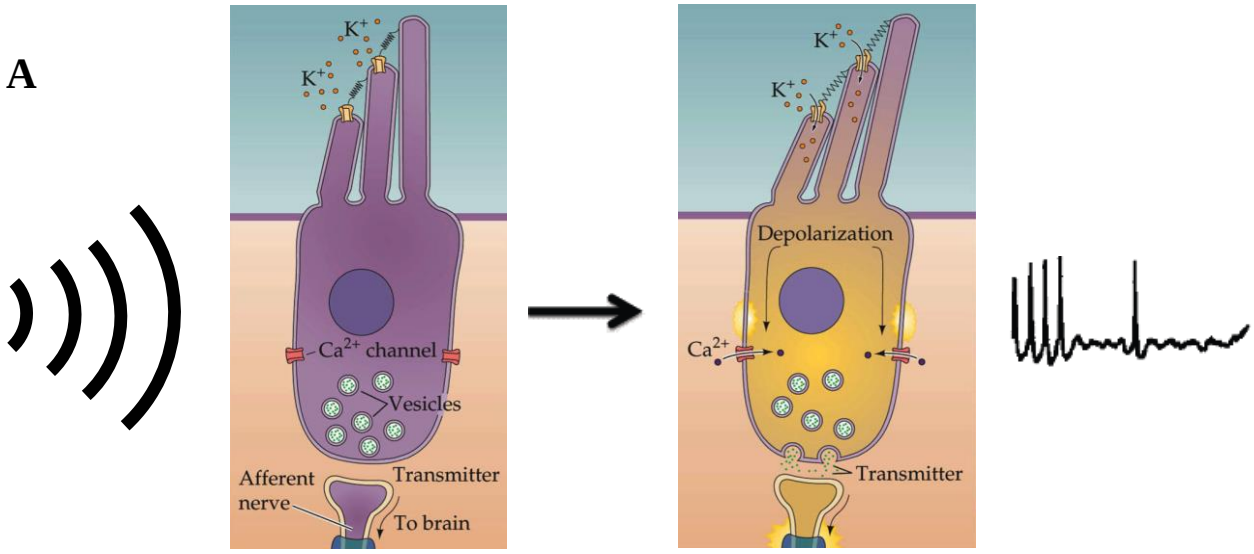

Figure 1.d The elements of mechanotransduction **A**) A mechanical stimulus acts upon the hair cell, causing a tensioning of the tip link that opens a transduction channel, and creates an electrical signal that can be translated by the brain[46] **B)** A transmission electron micrograph image from 1985 of a mammalian hair cell with a bundle of stereocilia on its apical end[47] **C)** A high-resolution scanning-electron microscopy image of the v-shaped structure of a bundle of stereocilia belonging to the guinea pig[48] **D)** A high-resolution, rapid-freeze, deep-etch electron microscopy image of the tip-link, constructed from cadherin-23 and protocadherin-15. This structure bridges the gap between adjacent stereocilia[49].

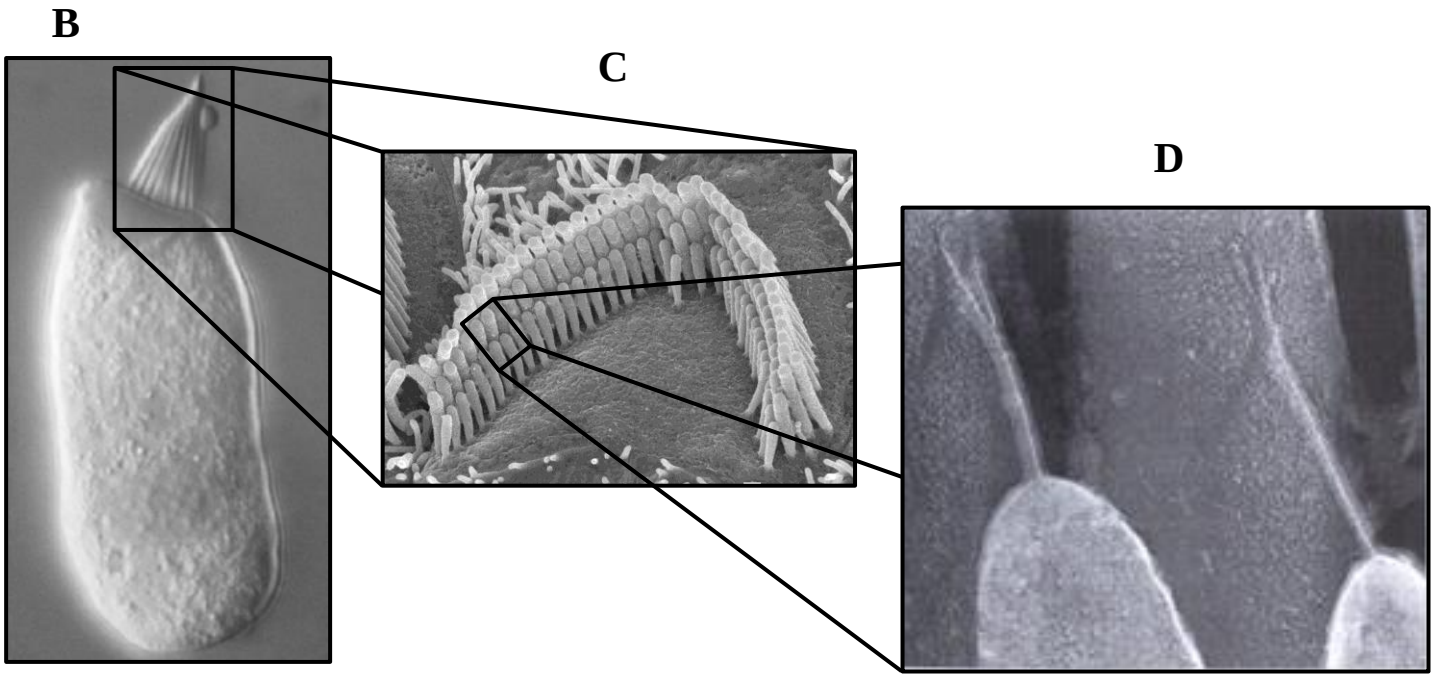

1.3 Introducing the Cadherin Superfamily of Cell-to-Cell Adhesion Proteins

To understand the unique role of the tip link protein's, CDH23 and PCDH15, I will briefly introduce the cadherin superfamily of cell-to-cell adhesion molecules. The cadherin family is responsible for the organization of cells into tissues and organs to regulate processes such as cell adhesion, morphogenesis, synapse formation, cell sorting/migration, pathological conditions such as cancer, and the development and function of more than 100 sensory cells[17]. These proteins are all defined by an approximately 110 residue β-fold domain, the common structural unit known as the extracellular cadherin (EC) domain. The EC domains tend to have similar amino acid compositions and are joined together via three calcium ions at conserved binding sites[18].

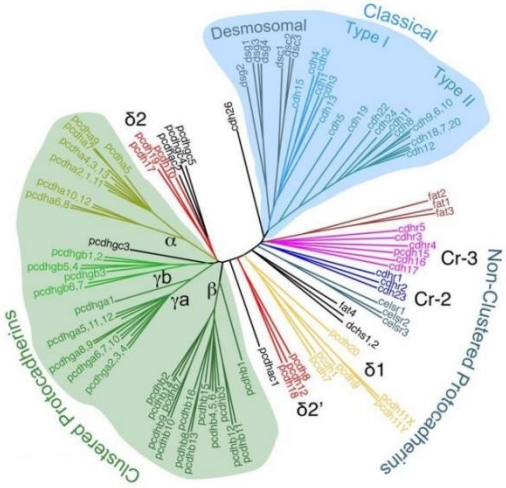

Figure 1.e The cadherin superfamily. CDH23 and PCDH15 belong to the Cr-2 and Cr-3 family, respectively[50]

Even with a common structural unit, the diversity in this family is indicated by sequence homology and domain structure analysis, allowing for a division into subfamilies including classical cadherins, desmosomal cadherins, seven transmembrane cadherins, protocadherins and other cadherin-related molecules. The cadherins are classified on an EC1 to EC3 basis in figure 1.e. Whereas the extensively studied classical cadherins contain a single-span transmembrane, five EC domains, and mediate adhesion by the "swapping" of opposite EC1 N-terminal β-strands via conserved tryptophan side chains fitting into hydrophobic pockets; other non-classical cadherins appear to have evolved distinct structural features and adhesive mechanisms including

CDH23 and PCDH15 that join in a novel interaction that is only recently beginning to be understood[17,19].

1.4 CDH23 and the Tip Link

The tip-link, composed of CDH23 and PCDH15[20,21], is the core component of hearing and much research has been conducted to elucidate its true purpose by understanding its molecular structure, elasticity, and deafness-related structural defects. The two proteins that form the tip-link are non-classical cadherins with single transmembrane domains and C-terminal cytoplasmic domains[22,23]. Both CDH23 and PCDH15 also have an unusually large number of EC repeats, twenty-seven and eleven respectively. These molecules share some fundamental similarities with classical cadherins, but important differences in structure and adhesive mechanisms make them unique.

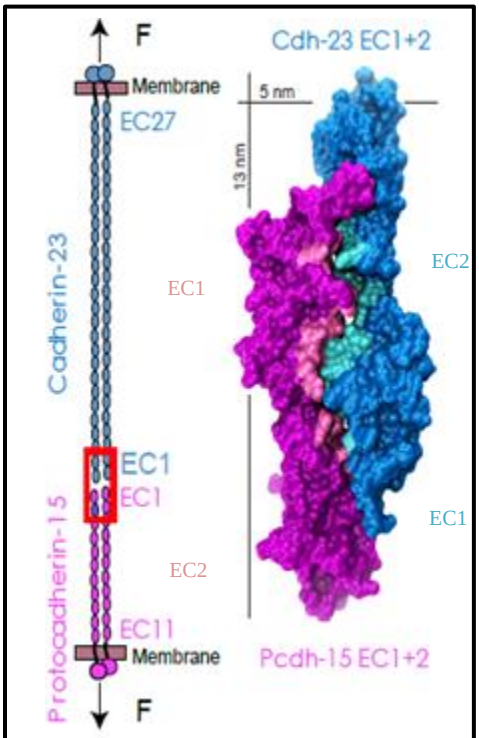

Figure 1.f The tip-link; red-box indicating solved EC repeats. VMD[51] representation of the extended handshake. Adapted from [28]

Tip links were first suggested to be involved in sensory transduction in 1984 when a group of researchers directed by Dr. Jim Pickles discovered an extensive array of cross-links between stereocilia, particularly the shorter stereocilium of one row giving rise to a single, upwards-pointing link which ran up to join the side of the adjacent, taller stereocilium of the next row[24]. To visualize the structure and what we know today as the tip link, both scanning and transmission electron microscopy were utilized. To provide

experimental evidence that this tip link was instrumental in hair-cell transduction, another group of researchers (Assad et. al., 1991) observed that stereocilia bundles treated with BAPTA, a Ca^{2+} chelating saline compound, abolished transduction currents and eliminated the tip link molecule for a few seconds[25].

To identify the protein(s) that constitute the tip link, researchers (Siemens et. al., 2004; Söllner et al., 2004) first illustrated that cadherin-23 was one possible candidate through studying mutations in its gene that cause deafness and age-related hearing loss. Supporting evidence arose from independent immunolabeling studies in both mice and zebrafish that placed CDH23 to the topmost portion of the tip link structure[26,27]. In a similar fashion, immunolabeling experiments identified PCDH15 in the mouse inner ear. With supporting evidence, researchers (Ahmed et. al., 2006; Kazmierczak et. al., 2007) were able to make the first claims that CDH23 forms the upper two-thirds and PCDH15 the bottom third of the tip link[20,21].

In 2010, Dr. Marcos Sotomayor was the first person to structurally elucidate the connection between CDH23 and PCDH15. The overall fold matched the well-known Greek key motif of classical cadherins and three Ca^{2+} ions were in a canonical relationship at the linker region between repeats EC1 and EC2 of each protein, but there are several novel structural features that illustrate the diversity among cadherin adhesion mechanisms[28]. Most distinctly, the two most amino-terminal cadherin repeats (EC repeats 1 and 2) of each protein interact to form an overlapped, antiparallel heterodimer that resembles an ‘extended handshake’ involving only four of the thirty-eight EC repeats that form the tip-link. In this arrangement, CDH23 and PCDH15 form a linear array of 38, 4 nm long, cadherin domains that are ~150 nm in length and capable of spanning the gap between adjacent stereocilium[29].

Although much knowledge has been elucidated about vertebrate mechanotransduction, the tip link is just one major piece to a puzzle that still holds some mystery. To this date, the structure that pulls open the mechanosensitive ion channel directly termed the "gating spring" and the channel itself remain at large. Specifically, many in the field debate whether or not the gating spring is the tip link itself or proteins other than CDH23 and PCHD15. It may be provided by proteins that connect the tip link to the channel or proteins that anchor the channel to the underlying actin core[30]. Mechanical measurements determined that the gating spring stiffness is approximately 1 mN/m[31,32], yet steered molecular dynamics (SMD) simulations of EC1 and EC1+2 carried out by Dr. Sotomayor predicted the tip link stiffness to be ~40-60 mN/m in the presence of Ca^{2+} and at a pulling speed of 0.1 nm/ns[33]. The different values generated for the gating spring stiffness, when comparing the mechanical pulling versus SMD simulations, is significant and a reason why scientists claimed the tip link was too rigid to serve as the gating spring. There could be a more elastic element yet to be discovered that serves as the gating spring and it is still possible that the tip link serves the purpose. Even though each EC repeat is closely related in sequence and canonical Ca^{2+}-binding sites are conserved, the SMD simulations only accounted for EC1+2 and there could be enough variability in the other 36 repeats to render the tip link more compliant and conducive to 1 mN/m.

1.5 Exploring an Unusual Calcium-Binding Site of CDH23

Experiments have shown that calcium (Ca^{2+}) depletion around hair cells results in elimination of the tip-link completely, only to reassume structure several hours after Ca^{2+} restoration. Molecular dynamics (MD) simulations to investigate the dynamics of the EC1+2 portion of E-cadherin in the presence and absence of Ca^{2+} confirm that apo-cadherin exhibits a

much higher flexibility than the Ca^{2+}-bound form[34]. Evidence from both simulations and electron microscopy studies on the E-cadherin molecule show that EC1+2 demonstrates a large and reversible conformational transition from a rod-like structure to a more globular assembly of the five subdomains upon Ca^{2+} depletion[35]. Not only are Ca^{2+} and Ca^{2+}-binding residues crucial for elasticity and function in classical cadherins, but MD simulations also suggest that the non-classical CDH23 EC1+2 molecules are stiff, with their molecular strength and interrepeat dynamics mediated by Ca^{2+} binding to highly conserved acidic residues.

I became interested in this project after a sequence alignment comparing amino acids of all 27 repeats of cdh23 indicated a single non-conserved Ca^{2+} binding site between EC12-13 in which an aspartate is replaced by a serine (Fig. 1.g B). The normal, conserved Ca^{2+}-binding site is referred to as DXD (aspartate [D]-any residue [X]-aspartate [D]) whereas this aspartate to serine [S] variation is referred to as the SXD site. Aspartate, an acidic amino acid, is suitable for coordinating a positively charged Ca^{2+} ion. Serine, referred to as a polar amino acid, may coordinate a Ca^{2+} ion but to an unknown extent. Each Ca^{2+} has multiple residues coordinating it, but exchanging an aspartate for a serine in one out of twenty seven conserved Ca^{2+}-binding motifs suggests that something unusual could be transpiring at this location. I am determined to understand how this variation in EC12-13 of cdh23 affects the rigidity and molecular strength of the tip link.

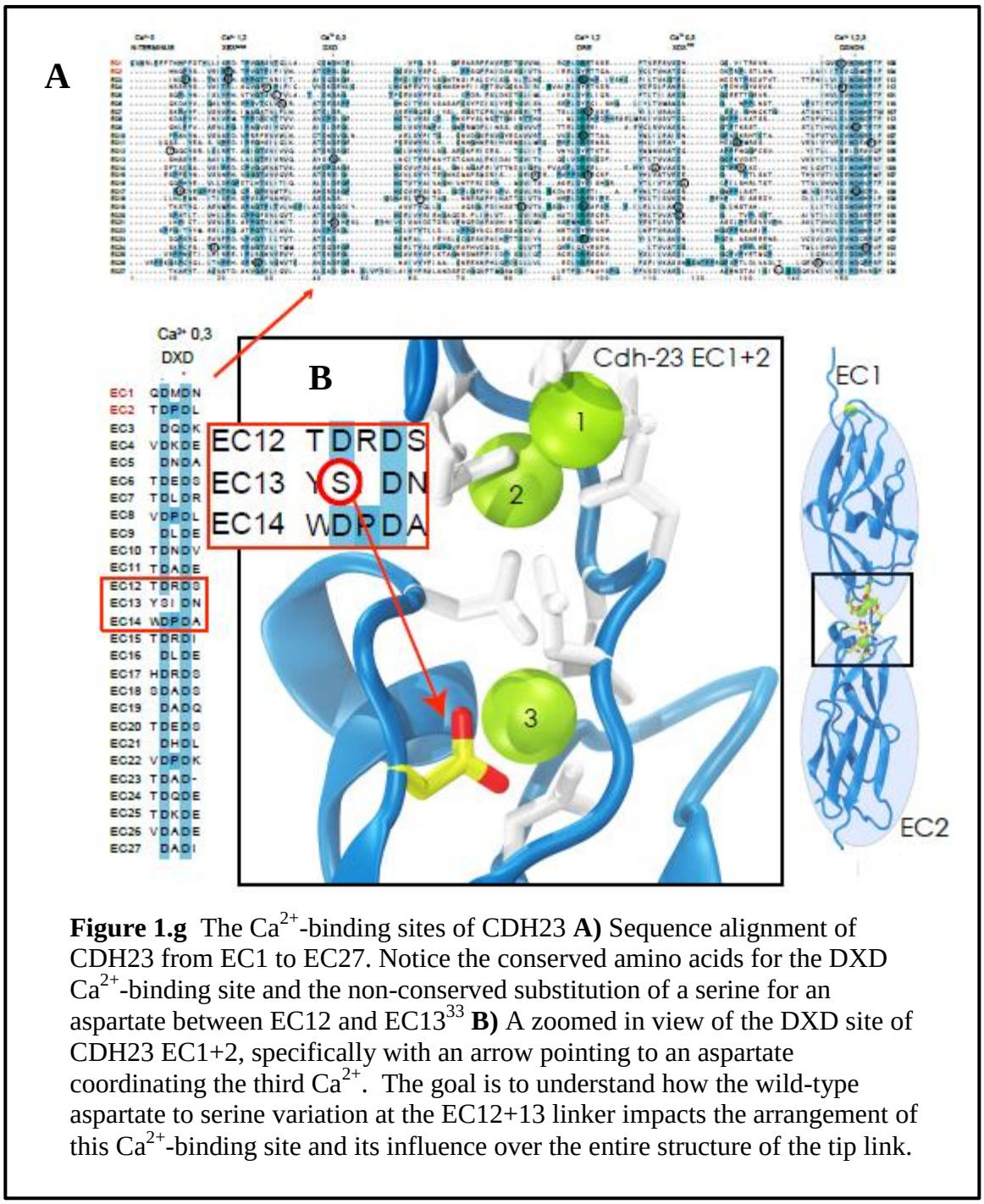

Figure 1.g The Ca^{2+}-binding sites of CDH23 **A)** Sequence alignment of CDH23 from EC1 to EC27. Notice the conserved amino acids for the DXD Ca^{2+}-binding site and the non-conserved substitution of a serine for an aspartate between EC12 and EC13[33] **B)** A zoomed in view of the DXD site of CDH23 EC1+2, specifically with an arrow pointing to an aspartate coordinating the third Ca^{2+}. The goal is to understand how the wild-type aspartate to serine variation at the EC12+13 linker impacts the arrangement of this Ca^{2+}-binding site and its influence over the entire structure of the tip link.

1.6 Linking Mutations in CDH23 to Deafness

As a student of American Sign Language (ASL) and one who can appreciate deaf culture from the outside, I can understand how some individuals suffering from a spectrum of hearing

loss will not refer to deafness as a disability, but as a cultural identification and linguistic minority. It is not that their lack of hearing "condemns them to a world of silence"[36], but that their lack of hearing enhances other areas of perception that allows them to live as contributing members of society. Deaf culture is alive and well, but with 90% of deaf children born to hearing parents, those who label deafness as a disability would have a point in reasoning that this individual is joining a familial and societal heritage that does not consider the inability to hear an integral part of its day-to-day functioning. The medical decisions that hearing parents must make for deaf children such as getting a cochlear implant or placing them in ASL programs at a young age, remains a controversial issue. The statement, "We do not live in a deaf community. We live in a high-rise apartment complex" often resonates with our hearing society[37].

Deafness is the most common form of sensory impairment, it can be produced from various sources, and results in a wide-spectrum of expressivity. With 500 million individuals predicted to be at risk for noise-induced hearing loss (NIHL), exposure to excessive noise through occupational exposures as musicians, farmers, construction workers, and other factors creates a complex disease which results from the interaction of genetics and environmental factors[38]. A common form and an area of interest for my research, deafness can arise from single gene mutations which can cause syndromic and nonsyndromic forms of deafness, as well as progressive and age-related hearing loss[39]. In fact, there are currently over 40 known missense mutations associated with deafness that target the EC domains of PCDH15 and CDH23[28]. I previously illustrated the importance of Ca^{2+} and Ca^{2+}-binding residues for the molecular strength and elasticity of the tip link and it seems logical that these same amino acid residues coordinating Ca^{2+} are often the targets of deafness mutations. Further analysis reveals a point mutation at SXD in which the remaining aspartate is mutated to an asparagine. The mutation,

D1341N, results in inherited nonsyndromic deafness or deafness characterized by no further abnormalities to other parts of the body.

After solving the structure of EC1+2 of CDH23, Dr. Sotomayor studied deafness mutations targeting Ca^{2+} motifs and he hypothesized based off MD simulations and Ca^{2+}-binding assays that mutations can affect CDH23 in possibly three ways. Pulling simulations of wild-type (WT) and mutant CDH23 EC1+2 with Ca^{2+} bound at sites 1-3 demonstrated comparable forces between the two, indicating that the mutant may be reducing CDH23's affinity for Ca^{2+} and changing CDH23's mechanical strength indirectly. Thus, CDH23 would suffer from a reduced mechanical strength at physiological Ca^{2+} concentrations of cochlear endolymph (20-40 μM). Alternatively, mutations can directly modify the Ca^{2+}-protein interactions to reduce the mechanical strength of the protein. The last hypothesis is that mutations may be impairing the *cis* and *trans* interactions between both homodimer CDH23-CDH23 interactions or heterodimer CDH23-PCDH15 interactions of the tip link by altering interrepeat orientation and dynamics[33]. Even though a lot of progress has been made in identifying gene mutations that cause hearing loss, we still know little about the mechanisms leading to disease and I would like to see if the D1318N mutation causes similar structural and functional defects as the D101G mutant Dr. Sotomayor studied. The overall goal is to provide an answer to this proposed question: If the tip link can be so susceptible to a single point mutation disrupting Ca^{2+} affinity, how is the wild-type SXD binding site arranged so that it maintains its functionality in comparison to DXD?

Chapter II: Engineering Fragments of CDH23

Does the variation from aspartate to serine alter the overall elasticity and rigidity of the EC12-13 junction? Utilizing the methodologies of X-ray crystallography, multiple Ca^{2+}-binding assays, single-molecule force spectroscopy, and MD simulations; the scientific evidence clarifying this question will someday be illuminated. However, to even be able to conduct these complicated experimental procedures and computational experiments, one must successfully transverse the central dogma with biochemical techniques to produce a sufficient quantity of properly-folded protein. I will go into depth on the common experiments that I, and most other members of The Sotomayor Research Group, utilize for the different constructs of the tip link; but, I cannot explain why some constructs behave and others do not, the time that some members wait for crystals to grow before they can even start thinking about solving a structure, or even the dreaded sight of a poor size-exclusion chromatography run in which 90% of the protein is aggregated and unusable. Before joining the lab I thought this was the easy part, but I have grown to respect the process and I find some hope in knowing that the next construct I try may be the one.

The ultimate goal of our lab is to elucidate the molecular mechanisms underlying vertebrate mechanotransduction and this is only possible through elucidating the tip link's molecular structure in its entirety. To understand the structure-function relationships, each member of the lab working on the tip link is assigned a portion of either CDH23 or PCDH15. From this approach, many members of the lab have had great success and discovered characteristics of the tip link that continue to evolve our knowledge of vertebrate hearing, such as domains of PCDH15 lacking Ca^{2+}-binding sites entirely. I chose to work with the non-conserved Ca^{2+}-binding site, SXD, between EC12 and EC13. To this end, I have engineered various DNA

constructs, variable numbers of EC repeats containing the area of interest, to work with ranging from two repeats up to five. I detail every construct I have created since joining the lab and at what point in the process towards structural determination I am at. In addition, this chapter will include the methodology and results for the cloning, expression, and purification of my constructs.

2.1 Cloning Various DNA Constructs Centered Around EC12 and EC13

All DNA fragments in this research were generated with template cDNA of CDH23 via PCR from either *Mus musculus* or *Homo sapien* sources and complementary primers of each construct were ordered from Sigma-Aldrich. *Homo sapiens* CDH23 was ordered as a synthetic gene from Bio Basic Inc. and *Mus musculus* CDH23 was obtained from U. Mueller at the Scripps Research Institute through Dr. David Corey at Harvard Medical School. The fragment constructs were designed by using the published structure of cadherin-23 EC1 and EC2 (Protein Data Bank code 4APX[28]) as a reference in conjunction with sequence alignments of CDH23 EC repeats to avoid disrupting predicted secondary structure features[33]. All primers included a short spacer sequence (5'-CCGCCG-3') and the sequence of NdeI and XhoI enzyme restriction sites (5'-CATATG-3' and 5'-CTCGAG-3', respectively) in addition to the complementary sequence of the desired region of the gene to be cloned. The DNA constructs and pET-21a(+) vector, an approximately 5,443 bp structure containing an ampicillin resistance gene, C-terminal histidine-tag, and an isopropyl β-D thiogalactopyranoside (IPTG) inducible T7 promoter, were digested with NdeI/XhoI and ligated together. With the recombinant DNA generated, the DNA plasmids were propagated by bacterial transformation via the DH5α *E. coli* strain. To verify successful replication of the DNA of interest, each plasmid was miniprepped for isolation from the bacterial competent cells, analytically digested to visualize appropriate DNA fragment sizes of both the

insert DNA and the pET-21a(+) vector on an agarose gel, and sequenced using the T7 promoter and terminator primers.

2.2 Protein Expression in *E. coli*

For over two decades, protein expression in the bacterium *E. coli* has been the most popular method for producing recombinant proteins. I expressed all CDH23 constructs used in this study in the BL21-CodonPlus (DE3)-RIPL competent cells that enable high-level expression of heterologous proteins, or those expressed in a species or cell type different from where it originates. In addition to containing a T7 polymerase gene that allows for high-level expression when induced with IPTG, the BL21-CodonPlus (DE3)-RIPL efficiency can be contributed to its engineered ability to contain extra copies of genes that encode the tRNAs that most frequently limit translation of heterologous proteins in *E. coli*, the rare codons. Utilizing the NIH Rare Codon Calculator[40] (RaCC) that screens for arginine (Arg), leucine (Leu), isoleucine (Ile), and proline (Pro), it was determined that the shortest construct I work with, a two repeat structure of CDH23 EC12+13, codes for seven rare codons altogether (3 Arg, 3 Pro, 1 Ile). With this pool of rare tRNAs provided by the competent cells, stalled expression is overcome and over-expression of the protein of interest can be completed.

The overall goal of bacterial expression from *E. coli* is to obtain milligram quantities of the desired protein that can be utilized for different experimental techniques. The first step involves transforming and plating the BL21 competent cells on an ampicillin (Amp) and chloramphenicol (Chlor) LB agar plate. The Amp is specific to the pET-21a(+) vector and the Chlor is specific to the BL21 competent cells. A starter culture of 20 mL Lysogeny Broth (LB) medium, 20 μL Amp (100 μg/mL), 20 μL Chlor (34 μg/mL), and one colony from the plate were

placed in a 37°C incubator and shaken at 225 rpm overnight for approximately 16-20 hours. After the required time period for sufficient bacterial growth, a 2 L large-scale culture of Terrific Broth (TB) medium that contained 2 mL of both Amp and Chlor was inoculated with the entire starter culture. The culture grew at 37°C until it reached an OD_{600} between 0.4 and 0.6, at which point IPTG was added to a final concentration of 100 μM and the temperature was adjusted to 30°C. After growing overnight, the culture was removed from the incubator, pelleted, and stored at -20°C for at least 12 hours.

2.3 Purification Under Denaturing Conditions

Recombinant proteins expressed in bacteria, CDH23 included, tend to form inclusion bodies, or highly aggregated protein normally formed in the cytoplasm[41]. To account for this and prevent protein degradation, purification under denaturing condition with Guanidine-HCl was utilized. To prepare for sonication, a total of approximately 60 mL of B Buffer is added to detach and suspend the frozen pellet ranging from 6-8 g. After sonication, the lysate was spun down in a JA-20 Beckman Hi-speed centrifuge at 20,000 rpm and 4°C for 30 minutes to remove cellular debris. Approximately 3 mL of Ni-sepharose high performance resin equilibrated with an equal volume of B Buffer was added to the protein-rich supernatant and nutated at 4°C for 1 hour in a batch incubation fashion. Due to the C-terminal Histidine tag engineered into all of the CDH23 constructs, the desired protein chelates the Ni-sepharose beads and remains bound until a competing molecule, imidazole, is used to elute it.

<u>Binding (B) Buffer</u>
20 mM Tris-HCl pH 7.5
10 mM $CaCl_2$
6 M Guanidine-HCl
20 mM Imidazole

<u>Elution (E) Buffer</u>
20 mM Tris-HCl pH 7.5
10 mM $CaCl_2$
6 M Guanidine-HCl
500 mM Imidazole

All supernatant is collected via centrifugation at 3,000 rpm/4°C, and loaded onto an SDS-PAGE gel for analysis (the following steps are detailed visually in figure 2.a). After nutation, the suspension of Ni-sepharose resin and B Buffer is spun down and the supernatant, denoted as the flow-through (FT), containing the majority of undesired cellular proteins is removed. With the CDH23 construct still bound to the Ni-sepharose resin, the mixture is washed with 30 mL additions of Buffer B followed by centrifugation and collection twice, in two successive rounds (denoted W1 and W2). To elute the desired CDH23 protein from the Ni-sepharose resin, 30 mL of E buffer containing a much higher concentration of imidazole is added, the suspension centrifuged, and the supernatant of denatured protein collected.

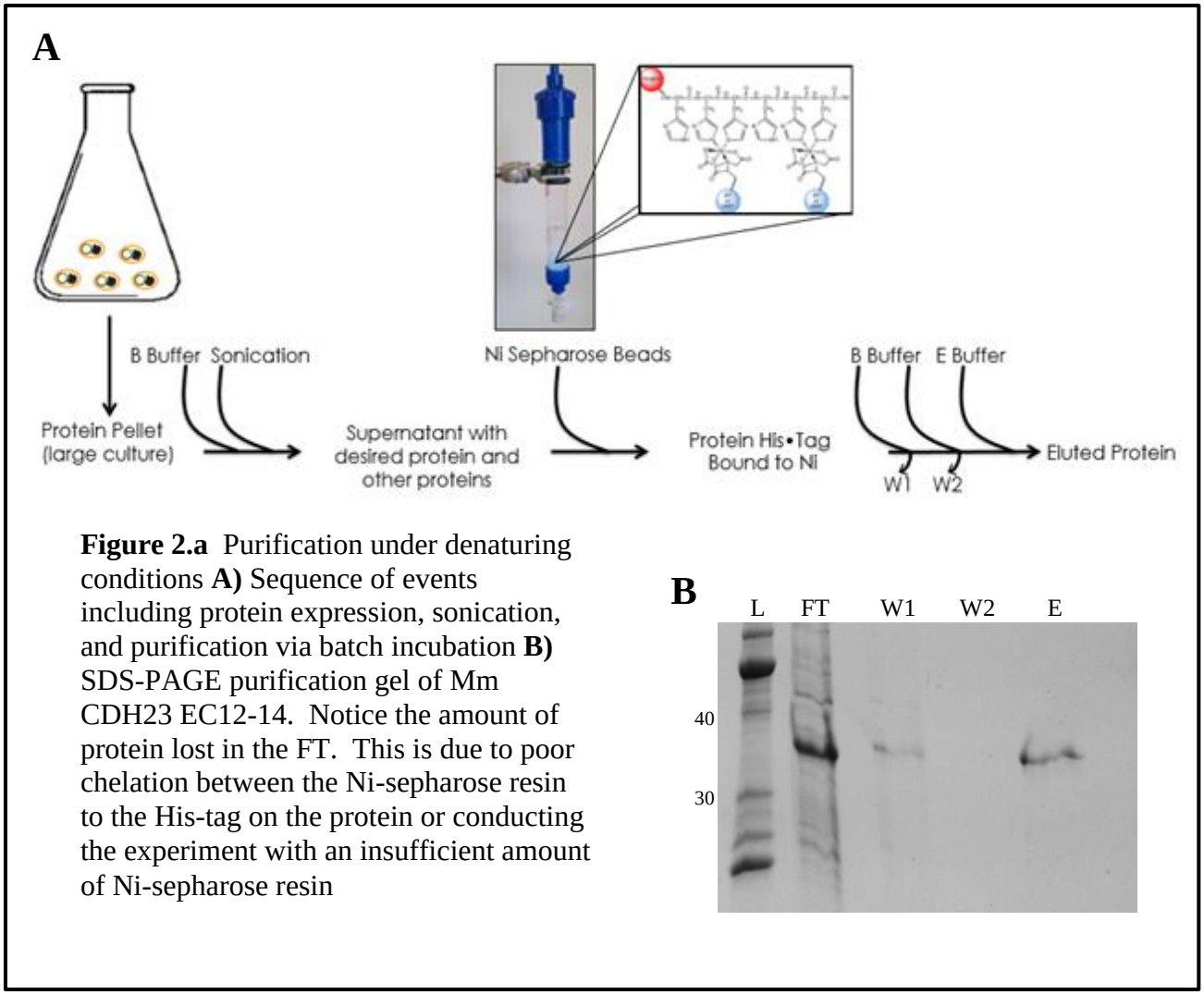

Figure 2.a Purification under denaturing conditions **A)** Sequence of events including protein expression, sonication, and purification via batch incubation **B)** SDS-PAGE purification gel of Mm CDH23 EC12-14. Notice the amount of protein lost in the FT. This is due to poor chelation between the Ni-sepharose resin to the His-tag on the protein or conducting the experiment with an insufficient amount of Ni-sepharose resin

2.4 Refolding and Separation via Size-Exclusion Chromatography

Dialysis Buffer
20 mM Tris-HCl pH 8.0
2 mM $CaCl_2$
150 mM NaCl
400 mM Arginine
SEC Buffer
20 mM Tris-HCl pH 8.0
2 mM $CaCl_2$
150 mM NaCl

The 30 mL elution of protein solution, confirmed to be 0.5<[CDH23]<1.0 mg/mL, was diluted further by separating into two conical vials; each with 15 mL protein solution, 15 mL E buffer, and 150 μL of DTT. The contents of each tube was pipetted into its own dialysis membrane and placed into the dialysis buffer at 4°C. The membranes were left in the buffer overnight to gradually remove the Guanidine-HCl until the desired protein construct refolded. The dialyzed solution was centrifuged at 20,000 rpm for 15 minutes at 4°C as a precautionary step to remove any precipitated protein. At this point, the clear solution of diluted protein is either well-folded or aggregated and the sample must be prepared for size-exclusion chromatography (SEC). A 10,000 MWCO polyethersulfone (PES) concentrator (Sartorius VIVASPIN 20) is utilized to concentrate the supernatant to either 2 mL or 5 mL, depending on the protein concentration and availability of a 5 mL SEC loop. Prior to running the protein on the SEC, the protein concentration ranged from 5-15 mg/mL.

SEC with the S200 Superdex 16/60 GL (GE Healthcare) was used to separate all protein constructs presented. This purification method allows for a separation of molecules according to differences in size and its high resolution fractionation makes it a suitable step to polish off our purification scheme. By using an SEC media that consists of a porous matrix of inert spherical particles (Fig. 2.b A&B), large molecules such as aggregated protein elute first while smaller molecules, the well-folded CDH23 constructs, with low hydrofluidic volumes enter the pores and elute last allowing for efficient separation into a 96-well block. The SEC column is equilibrated with SEC buffer, the concentrated protein solution is filtered using a 0.22 μm PES membrane

(Sartorius Minisart®), and it is then loaded onto a 5-mL loop for separation. The spectrum consists of an x-axis of mL of solution eluted and a y-axis of absorbance, measuring the protein abundance via UV absorbance at 280 nm (Fig. 2.b D). By identifying the separate peaks on the spectrum, one can select appropriate fractions to be analyzed on a Coomassie-stained SDS-PAGE gel to access the purity of the CDH23 fragment of interest.

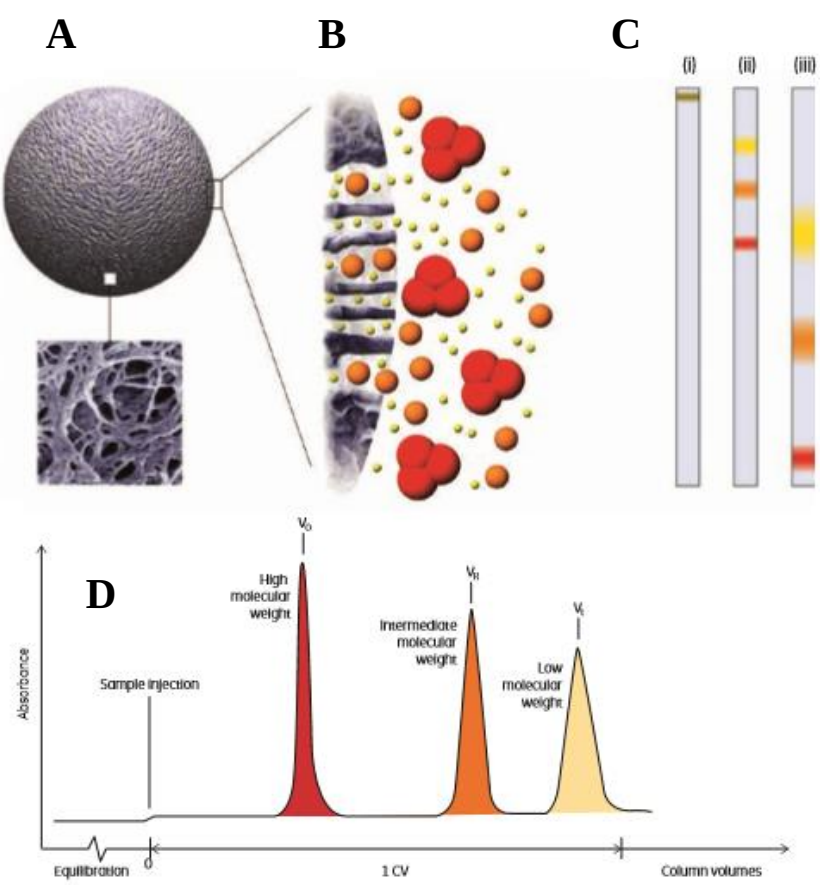

Figure 2.b Size-exclusion chromatography **A)** SEC bead with an electron microscopic enlargement **B)** Cartoon illustration of molecules diffusing into bead pores **C)** Stages of separation (i) sample applied to column at t=0 (ii) smallest molecule (yellow) is more delayed than largest molecule (red) (iii) largest molecule will elute first from the column. *Notice relationship between C) and D) with band broadening corresponding to peak width **D)** Illustration of SEC spectrum. V_o is void volume (~30% of total column volume) and V_t is one total column volume. Adapted from [52]

2.5 Results: Cloning, Purification, and Separation of Wild-Type CDH23 Constructs

A

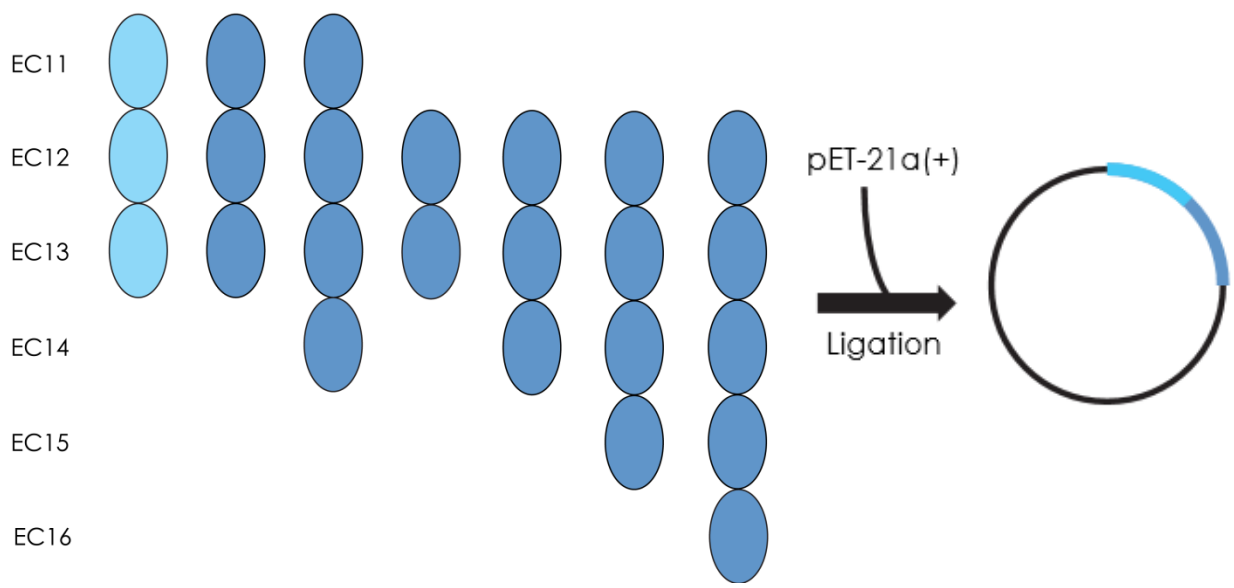

Figure 2.c Wild-type constructs of CDH23 **A)** Focused on a Ca^{2+}-binding site between EC12+13, both human (Hs) and mouse (Mm) constructs were ligated into the pET-21a(+) vector and expressed to study the location of interest. Hs CDH23 EC11-13 failed to refold, Mm CDH23 EC11-13 and EC11-14 are in progress, and the results for Mm CDH23 EC12+13, EC12-14, EC12-15, and EC12-16 are below. **B)** Information on the constructs illustrated above

B

Construct	Residues	# of Residues	Molecular Weight (Da)
Hs EC 11-13	N1075 to N1391	317	35,164.20
Mm EC 11-13	N1075 to N1389	315	34,808.90
Mm EC 11-14	N1075 to N1500	426	46,743.10
Mm EC 12+13	E1181 to N1389	209	22,788.50
Mm EC 12-14	E1181 to N1500	320	34,722.70
Mm EC 12-15	E1181 to N1605	425	46,294.50
Mm EC 12-16	E1181 to N1717	537	58,497.00

A

✓ Yes
× No
◔ In progress
☐ Not attempted

Construct	DNA	Expression	Refolding	Purification (SEC)	Concentrating	Crystal	Diffraction	Structure
Hs CDH23 EC11-13	✓	✓	×					
Mm CDH23 EC11-13	✓	◔	☐	☐	☐	☐	☐	☐
Mm CDH23 EC11-14	✓	◔	☐	☐	☐	☐	☐	☐
Mm CDH23 EC12+13	✓	✓	✓	✓	✓	✓	✓	
Mm CDH23 EC12-14	✓	✓	✓	✓	✓	✓	✓	
Mm CDH23 EC12-15	✓	✓	✓	✓	✓	×		
Mm CDH23 EC12-16	✓	✓	✓	✓	✓	×		

Figure 2.d A) This chart illustrates the progress of each wild-type CDH23 construct to date **B)** A sequence alignment of EC repeats for the entire Hs CDH23 protein used for labeling residues (Fig. 2.c B) in this thesis[33]. Please note that the residues comprising the signal sequence before EC1 are omitted and that the black circles indicate mutations causing hereditary deafness. Due to the sequence similarity between Hs and Mm CDH23, this sequence alignment can be used to label amino acids in the Mm protein as well.

B

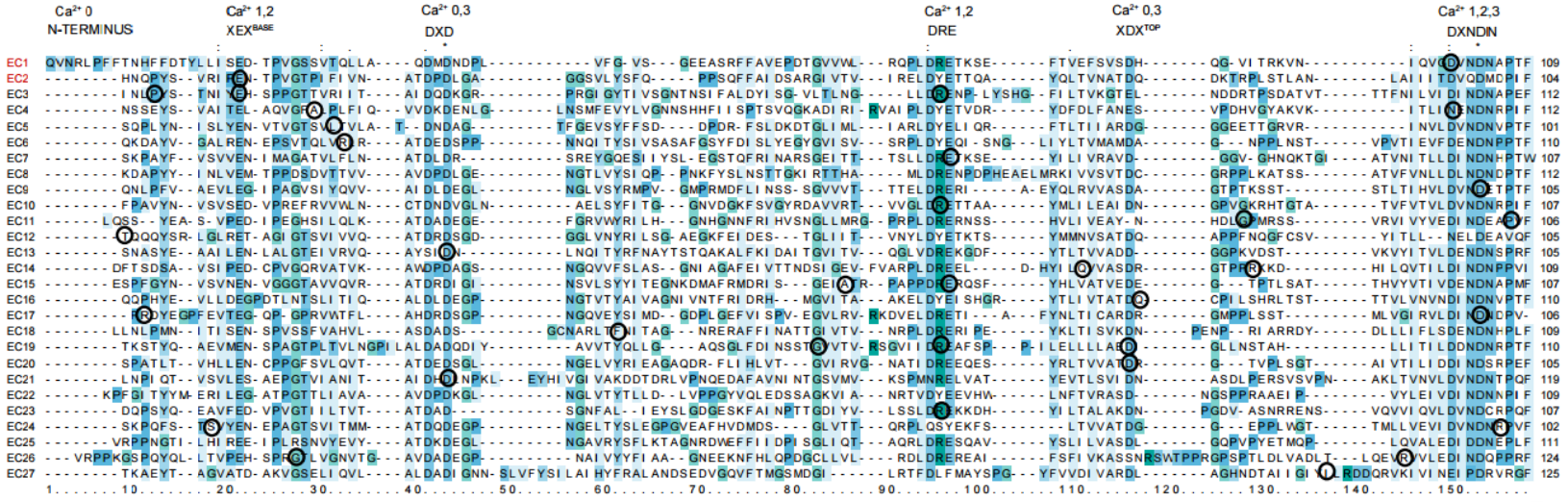

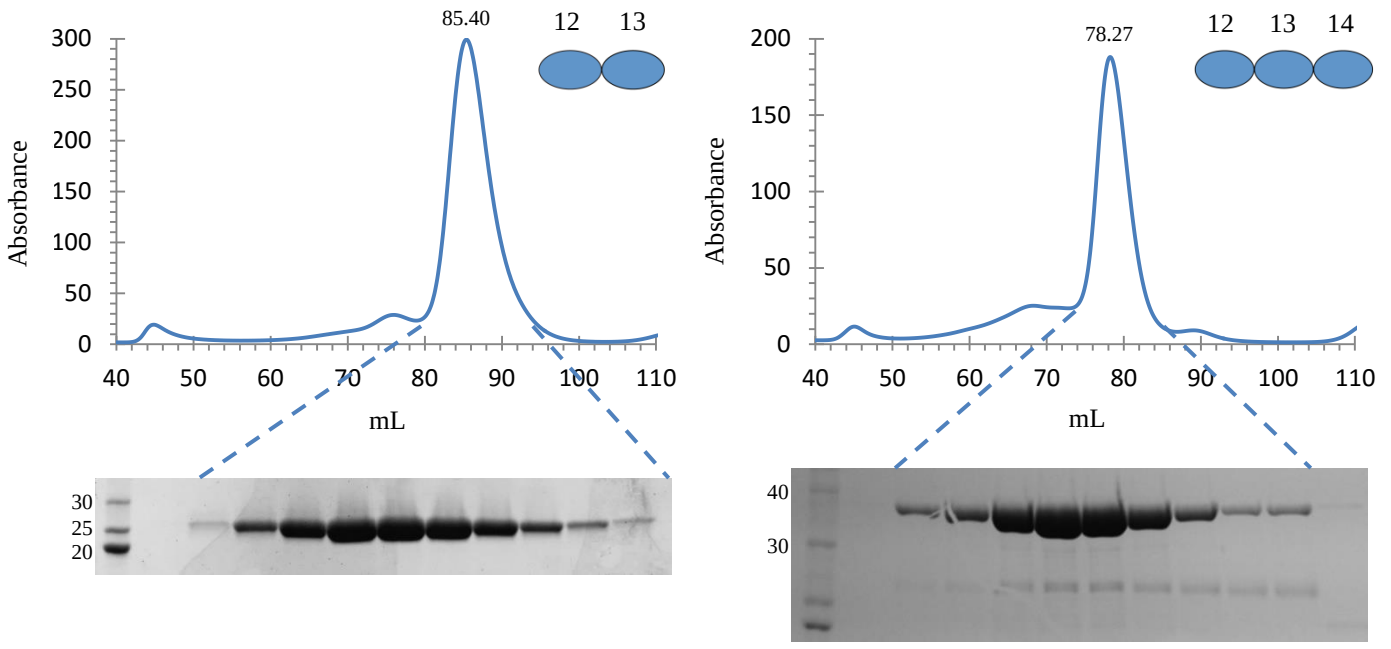

Figure 2.e SEC data for Mm CDH23 EC12+13, EC12-14, EC12-15, and EC12-16 with SDS-PAGE gels for validation. All constructs were refolded with the same dialysis buffer [20 mM Tris-HCl pH 8.0, 2 mM $CaCl_2$, 150 mM NaCl, 400 mM Arginine] overnight and run through the column with the same SEC buffer [20 mM Tris-HCl pH 8.0, 2 mM $CaCl_2$, 150 mM NaCl]

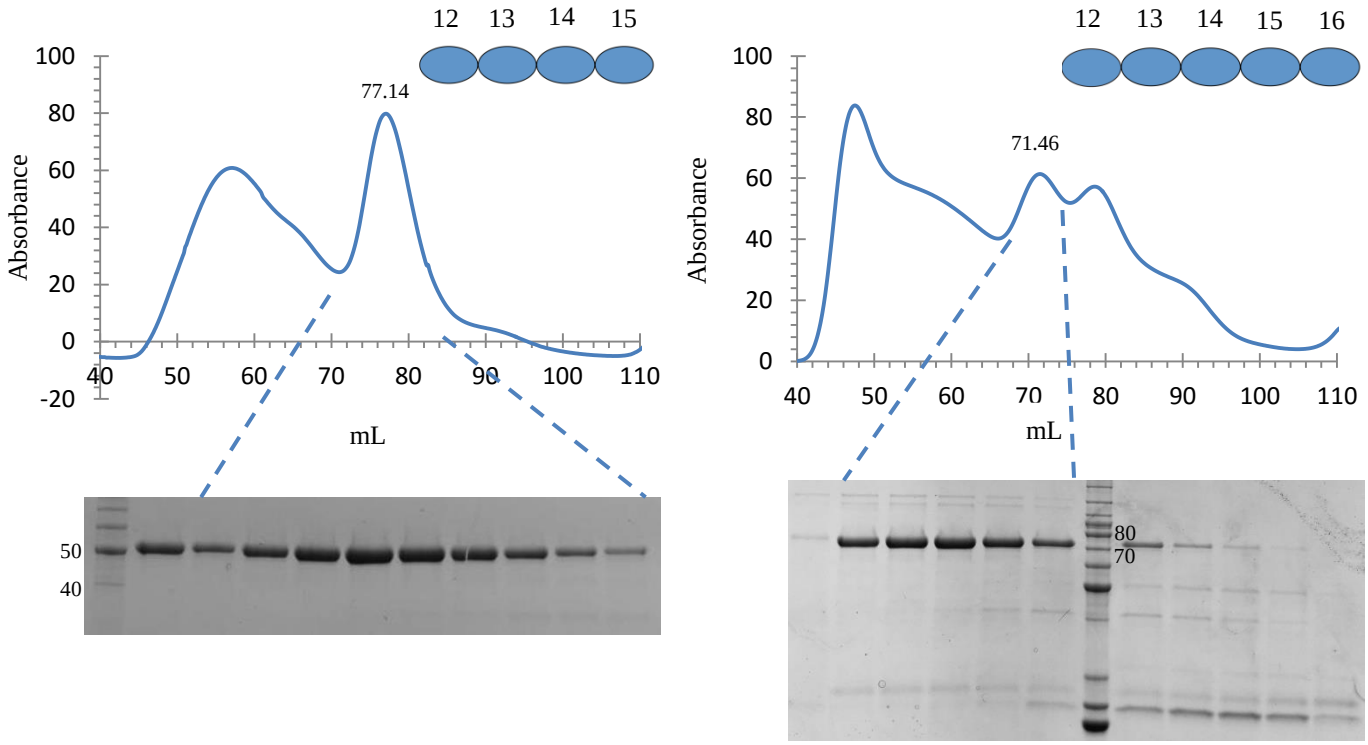

2.6 Conclusions

Obtaining purified, well-folded protein is an obstacle for many that often requires significant time and problem solving strategies to overcome. I experienced my fair share of frustration as I spent a good portion of one semester and a month of summer unsuccessfully trying to force the Hs CDH23 EC11-13 and Mm CDH23 EC12-14 constructs to refold. After giving up on the Hs construct, a bit of luck, and an elongated N-terminal addition to the protein; it became evident that Mm CDH23 EC12-14 refolds with a standard dialysis buffer that had previously been successful for other group members working with cadherins. Since this discovery approximately four semesters ago, I have had varying levels of success refolding and separating all Mm CDH23 constructs ranging from two (EC12+13) to five (EC12-16) EC repeats. Capable of producing sufficient quantities of protein for a multitude of constructs, I have been able to set many crystal trays with different constructs in pursuit of deciphering a molecular structure of CDH23 around my location of interest.

Before I present my protein crystallization and X-ray crystallography data, I want to hone in on the importance of site-directed mutagenesis and how I was able to generate additional mutant constructs (both engineered and diseased) to perform assays that test for Ca^{2+}-binding affinity. I will begin in a similar fashion to this chapter by introducing the methodology as well as categorizing the mutant constructs and showing SEC data. Next, I will present data from a trypsin sensitive assay and differential scanning fluorimetry (DSF) to evaluate protein stability via fluorescence.

Chapter III: Designing Engineered and Diseased CDH23 Mutants for Analysis

It is easy to be consumed by both the excitement and disappointment that is X-ray crystallography; a technique that relies on testing any and all combinations of buffer components to find the one that grows well-diffracting protein crystals. This focus on one area of research distracted me from other methods that could potentially provide the same information I was seeking, just in a different form. Instead of visualizing the SXD Ca^{2+}-binding site through structural determination, perhaps I could perform an assay to measure Ca^{2+}-binding and quantitatively analyze how this non-conserved site influences protein stability. With this idea, I turned to site-directed mutagenesis to create both engineered and diseased CDH23 constructs.

There are many reasons to create specific DNA alterations and one of them is to perturb a gene and analyze its subsequent activity. For CDH23, site-directed mutagenesis provides an opportunity to alter the WT EC12+13^{S1316} (SXD) construct into an engineered, EC12+13^{S1316D} (DXD), and a deafness, EC12+13^{D1318N} (SXN), mutant. Creating mutations into the EC12+13 SXD site is insightful, but the sequence homology between all twenty-seven EC repeats of CDH23 also provides an opportunity to build the SXD site of interest into a construct that has previously been structurally elucidated such as EC1+2. The advantage lies in the fact that we know how to crystallize this construct and the disadvantage arises from the significant difference in amino acid composition between EC1+2 and EC12+13 (~28% sequence identity), despite our knowledge that all EC repeats are generally conserved in terms of structure.

Regarding the non-conserved SXD binding site in only one-out-of-twenty seven EC repeats, I hope to illuminate how the aspartate to serine variation maintains the tip-links functionality and at what cost. Could it impact the rigidity of the tip-link enough to introduce a kink into what is proposed to be a linear structure? Regarding the SXN binding site, I want to

know how one single amino acid alteration can have as drastic of a result as deafness. Is the non-conserved SXD binding site already weak enough compared to the conserved DXD binding site that losing one more Ca^{2+}-binding residue is too much to handle? With these constructs, I can combine X-ray crystallography and Ca^{2+}-binding assays to holistically analyze the three and answer the proposed questions that I have.

3.1 Site-Directed Mutagenesis of CDH23 EC1+2, EC12+13 and EC12-14

Variant constructs were generated with the QuikChange Lightning Site-Directed Mutagenesis Kit from Agilent. The procedure utilizes a supercoiled double-stranded DNA vector, an insert of interest, and two mutant primers created via the Agilent primer design tool. Each primer is complementary to one strand and encodes the missense mutation of interest that will generate a plasmid containing one different codon compared to the parental strand after the temperature cycling of PCR is completed. Bacteria perform DNA methylation so the amplified product is treated with the *Dpn I* endonuclease that is specific for methylated and hemimethylated DNA which will digest the parental strand and not affect the mutation-containing synthesized DNA. The newly synthesized DNA is used to transform XL10-Gold competent cells which are lysed via sonication, the new vector was purified using the QIAGEN

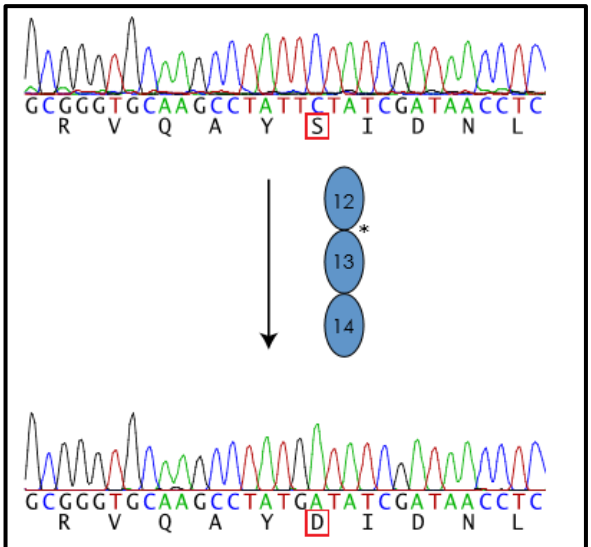

Figure 3.a Site-Directed Mutagenesis to create CDH23 EC12-14^{S1316D} confirmed via sequencing

Miniprep kit, and the desired DNA sequenced. Please refer to Chapter 2 for details on the expression and purification of CDH23 mutant constructs.

3.2 Trypsin Sensitivity Assay

Refolded protein of CDH23 EC1+2, EC12+13, and EC12+13^{S1316D} in SEC buffer [20 mM Tris-HCl pH 8.0, 2 mM $CaCl_2$, 150 mM NaCl] were diluted to approximately 3 mg/mL. Calcium is everywhere and the success of this experiment is contingent on decalcifying the protein to be used, F-buffer [10 mM MOPS pH 7.5, 100 mM KCl], trypsin, and any materials the assay reagents will be in contact with. For this reason, Chelex resin (Chelex 100) is used to remove all Ca^{2+} from solution so that the final concentration of Ca^{2+} is from the desired amount added.

F-buffer is separated into two 50 mL conical vials, 2% chelex resin (2 g/100 mL) is added, and the solution is nutated for two days. The protein solution and trypsin, 3 mg dissolved in F-buffer with 2 mM HCl, is chelated the day the experiment is to be conducted. To ensure that the free Ca^{2+} concentration is less than 20 nM, the chelated protein and F-buffer is calibrated against different calcium standards with Fura-2 (25 ng/µL) by measuring the absorbance maxima from ~348 nm to ~355 nm.

With the protein at the desired concentration and all substances decalcified, the experiment can be conducted by adding all reagents (Fig. 3.b) to a 96-well plate. A gradient of Ca^{2+} concentrations are utilized to visualize at which point the protein is not sufficiently protected from trypsin degradation. Notice that 0.5 M EGTA, a metal ion chelating agent with a high affinity for Ca^{2+}, is added at 0 µM Ca^{2+} so the protein should be fully degraded. Also, a 1600 µM Ca^{2+} sample at the end of the Ca^{2+} gradient acts as another control and the protein

should not be digested because no trypsin is added. Between these two extremes, a shift from degraded to intact protein should be visible on the SDS-PAGE gel.

[Ca^{2+}] (μM)	**0**	**16**	**32**	**64**	**128**	**256**	**320**	**480**	**800**	**1600**	**1600**
protein	46	46	46	46	46	46	46	46	46	46	46
F-buffer	0	0	0	0	0	0	0	0	0	0	2
$CaCl_2$	0	2	2	2	2	2	2	2	2	2	2
0.5 M EGTA	2	0	0	0	0	0	0	0	0	0	0
Trypsin	2	2	2	2	2	2	2	2	2	2	0
Total (μL)	**50**	**50**	**50**	**50**	**50**	**50**	**50**	**50**	**50**	**50**	**50**

The reaction time can range from 30 min to 90 min and can be conducted at room temperature or 37°C. After the allotted time, the reaction is quenched with 2 μL of PMSF, a trypsin inhibitor, and the separate wells are boiled after addition of 17 μL of SDS loading dye. Multiple SDS gels (4% stacking/20% resolving) were casted and the eleven reactions covering the spectrum of Ca^{2+} concentration were run for analysis.

3.3 Differential Scanning Fluorimetry

Whereas the trypsin sensitive assay provides comparative data on Ca^{2+}-binding affinity, Differential Scanning Fluorimetry (DSF) determines the structural stabilities of protein variants with the melting temperature (T_m), the midpoint of the protein unfolding transition[42]. Stable proteins have a higher T_m than unstable proteins and are less susceptible to unfolding and denaturation than their counterparts. This method is high-throughput, uses a very small amount of sample, and it is relatively inexpensive; it utilizes a real-time PCR machine to heat up a 96-well plate that can contain up to 96 different samples. DSF is based on monitoring the binding of a discriminating hydrophobic dye, SYPRO® Orange, to the protein of interest over a

temperature range due to the protein unfolding into a molten globule or thermal denaturation intermediate (Fig. 3.b).

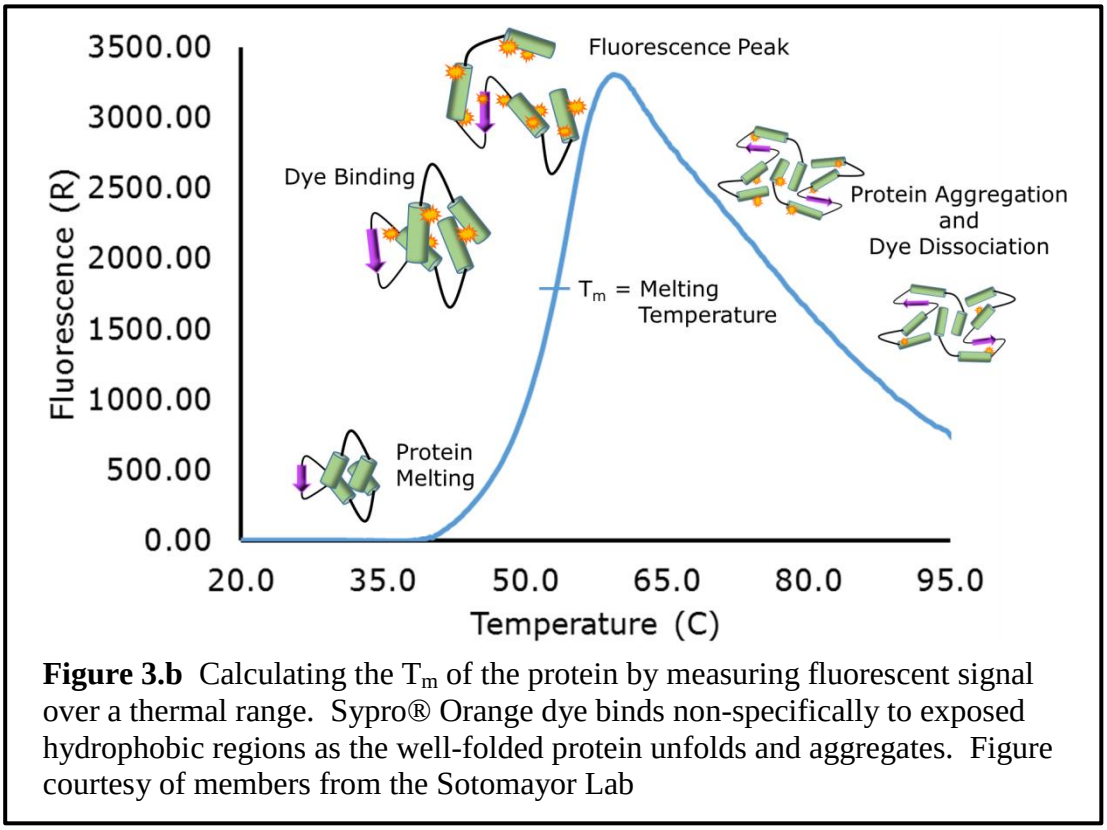

Figure 3.b Calculating the T_m of the protein by measuring fluorescent signal over a thermal range. Sypro® Orange dye binds non-specifically to exposed hydrophobic regions as the well-folded protein unfolds and aggregates. Figure courtesy of members from the Sotomayor Lab

After completion of site-directed mutagenesis and the techniques outlined in Chapter 2 concluding with SEC, the well-folded protein is diluted to a concentration of 0.3 mg/mL. Next, SYPRO® Orange is added to the protein solution and dispensed into a 96-well plate in triplicate. The tray is placed into a real-time PCR machine and heated from 10°C to 95°C for 425 cycles, the temperature increasing by 0.2°C per cycle. During this interval, the fluorescent changes are measured for wavelength of emission at 575 nm. The hydrophobic dye binds non-specifically and the fluorescence signal of the sample sharply increases as the protein unfolds, exposing hydrophobic regions to the polar environment.

3.4 Results: Cloning, Purification, and Separation of Mutant CDH23 Constructs

A

Mm CDH23 EC1+2 D135S	✓	✓	✓	✓	✓	✓	✓	◷
Mm CDH23 EC12+13 S1316D	✓	✓	✓	✓	✓	✓	✓	◷
Mm CDH23 EC12+13 D1318N	✓	✓	✓	✓	✓	✓	✓	
Mm CDH23 EC12-14 S1316D	✓	✓	✓	✓	✓	✓	×	

✓ Yes
× No
◷ In progress
☐ Not attempted

B

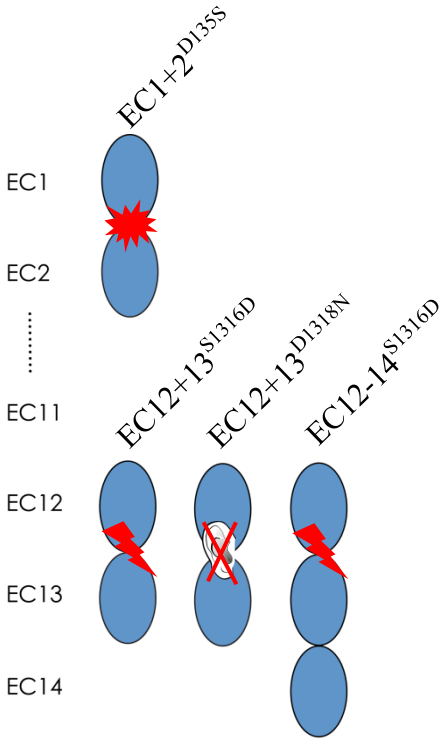

Figure 3.c Mutant constructs of CDH23 **A)** The progress of each mutant CDH23 construct to date **B)** Miniprepped WT DNA in the pET-21a(+) vector was altered with the Quikchange Lightning Site-Directed Mutagenesis Kit and the resulting mutant DNA was purified and isolated for use. This method was used to produce engineered ($EC1+2^{D135S}$, $EC12+13^{S1316D}$, $EC12-14^{S1316D}$) and deafness ($EC12+13^{D1318N}$) constructs **C)** Information on the constructs illustrated above

C

Construct	Residues	# of Residues	Molecular Weight (Da)
Mm EC $1+2^{D38S}$	Q1 to D205	205	22,584.10
Mm EC $12+13^{S1316D}$	E1181 to N1389	209	22,816.50
Mm EC $12+13^{D1318N}$	E1181 to N1389	209	22,787.50
Mm EC $12-14^{S1316D}$	E1181 to N1500	320	34,750.70

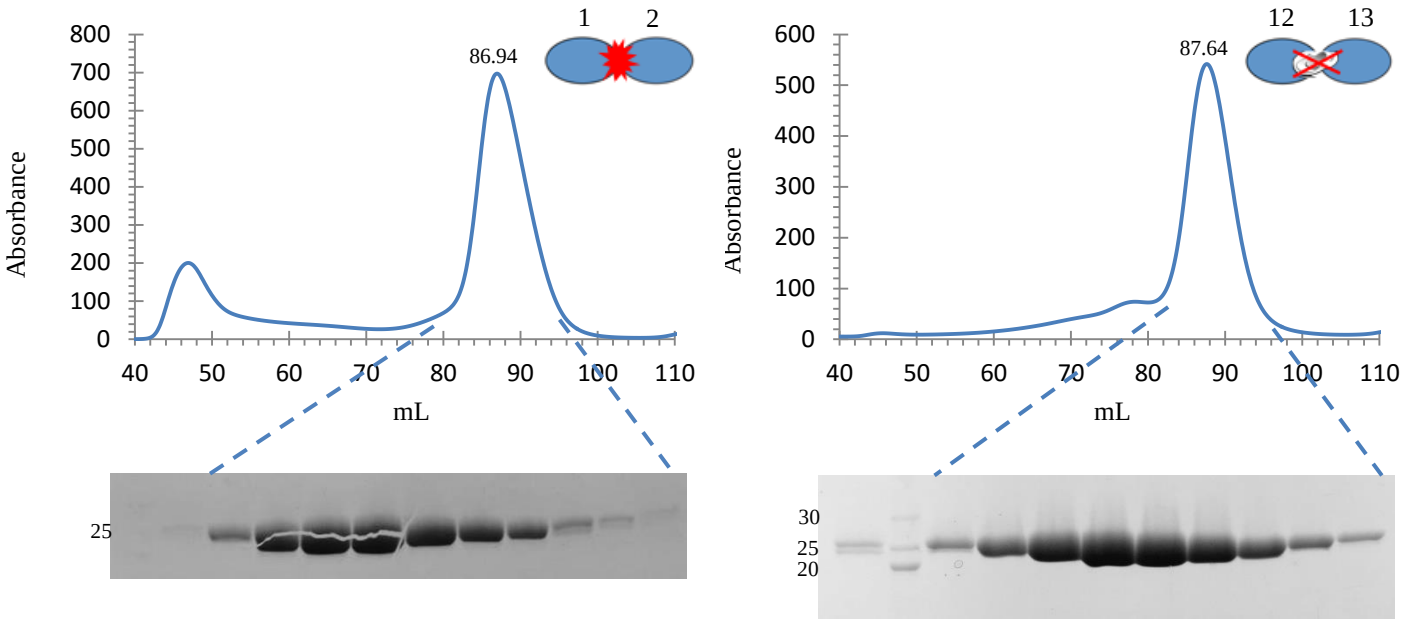

Figure 3.d SEC data for Mm CDH23 EC1+2^{D135S}, EC12+13^{D1318N}, EC12+13^{S1316D}, and EC12-14^{S1316D} with SDS PAGE gels for validation. All constructs were refolded with the same dialysis buffer [20 mM Tris-HCl pH 8.0, 2 mM $CaCl_2$, 150 mM NaCl, 400 mM Arginine] overnight and run through the column with the same SEC buffer [20 mM Tris-HCl pH 8.0, 2 mM $CaCl_2$, 150 mM NaCl]

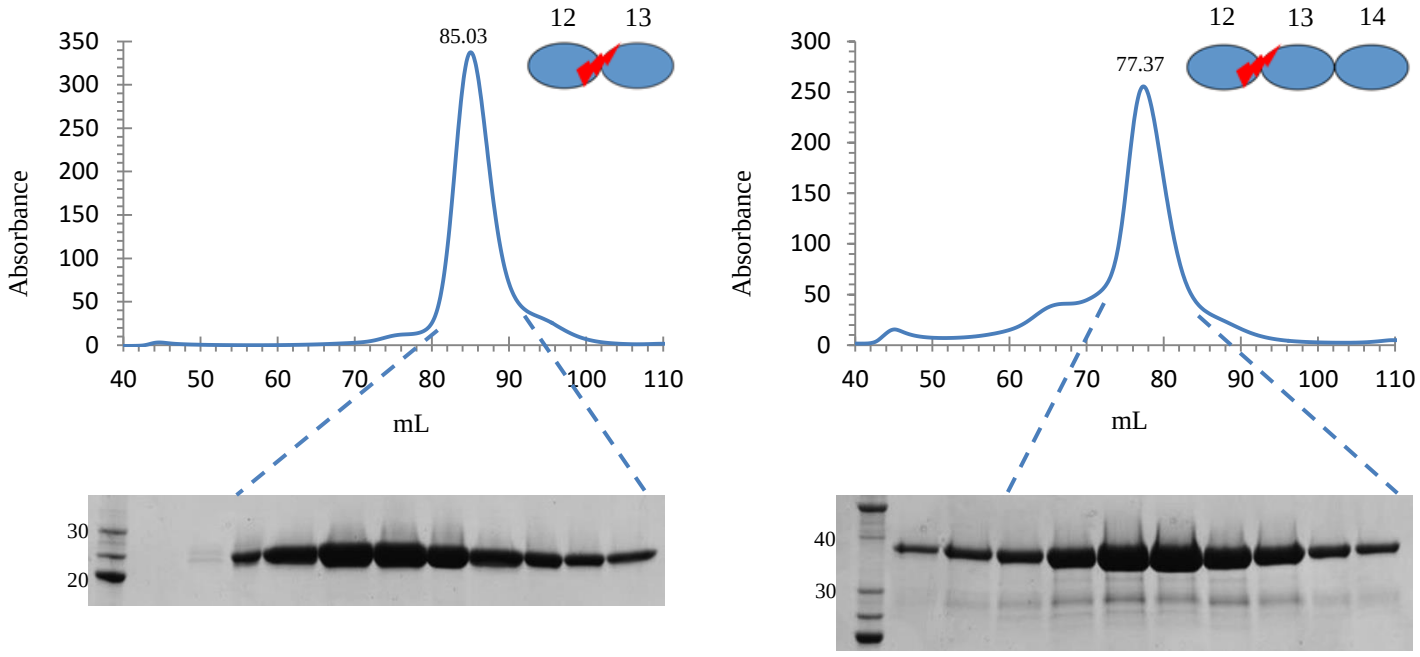

3.5 Results: Trypsin Sensitivity Assay Analysis

Trypsin cleaves cadherins and all proteins at the carboxyl side of the amino acids lysine and arginine unless inhibited by divalent cations such as Ca^{2+}. The protein variant that has a higher affinity for Ca^{2+} will require a lower concentration of additional Ca^{2+} to protect it from the trypsin and vice versa. Past trypsin sensitive assay experiments have tested the Ca^{2+}-binding affinity between wild-type CDH23 EC1+2 and a known deafness mutation that was believed to cause a decrease in cadherin stability by reducing its affinity for Ca^{2+} (Fig 3.g). I will use a similar approach.

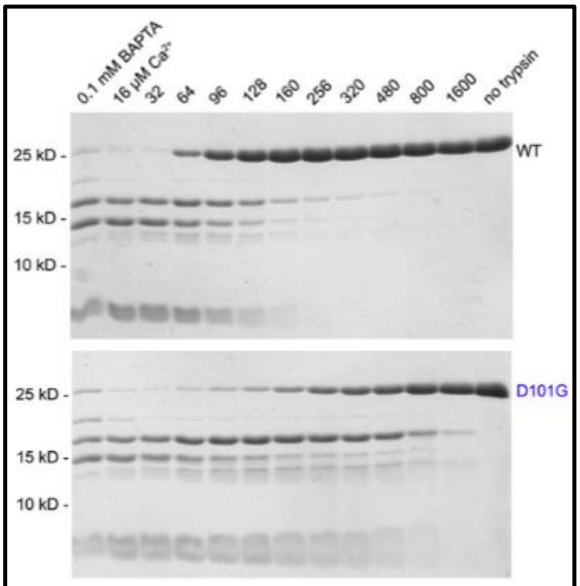

Figure 3.e Trypsin assay of CDH23 EC1+2 and EC1+2^{D101G} from [33] that served as the inspiration and protocol for my own. The WT protein requires much less Ca^{2+} to protect it from trypsin digestion, indicating a greater Ca^{2+}-binding affinity.

There are several outcomes possible in these experiments, but I want to focus on two. Result 1, both the wild-type and mutated version produce similar binding affinities postulating an insignificance in residue coordination at the SXD site. Result 2, the mutated version outperforms the wild-type thereby suggesting that variation from aspartate to serine does indeed have some implications in physiological context.

A

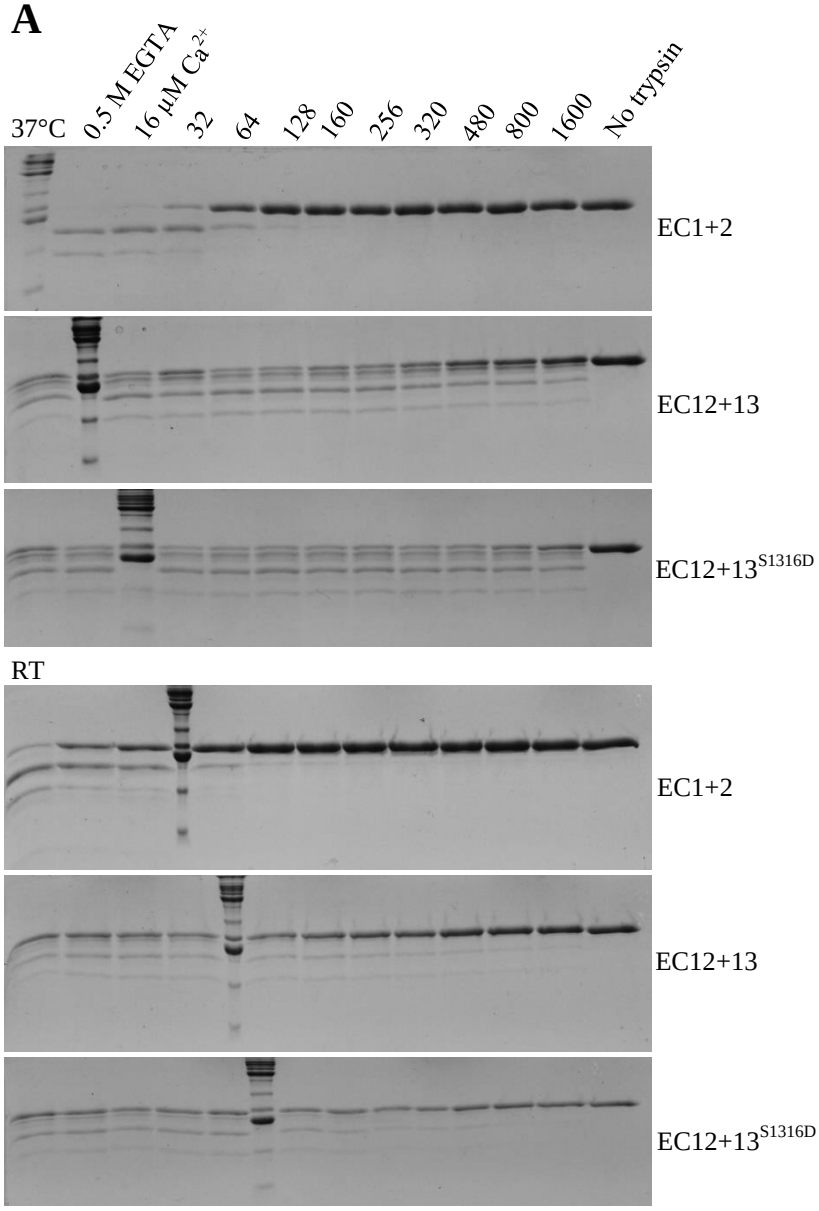

Figure 3.f The results of a trypsin assay (t=30 min) **A)** The proteins of interest (Mm CDH23 EC1+2, Mm CDH23 EC12+13, and Mm CDH23 EC12+13^{S1316D}) are analyzed on an SDS-PAGE gel. The top and bottom experiments were conducted at 37 °C and room temperature (RT), respectively. Notice how both of the EC1+2 intact protein bands at ~25 kDa increase in proportion along the Ca^{2+} concentration gradient from 0-1600 µM. This allows for quantitative measurements by measuring the intensity of the band with ImageJ **B)** Graphing the normalized intensities for EC1+2 against the Ca^{2+} concentration gradient and fitting the spectrum to obtain the effective K_d

B

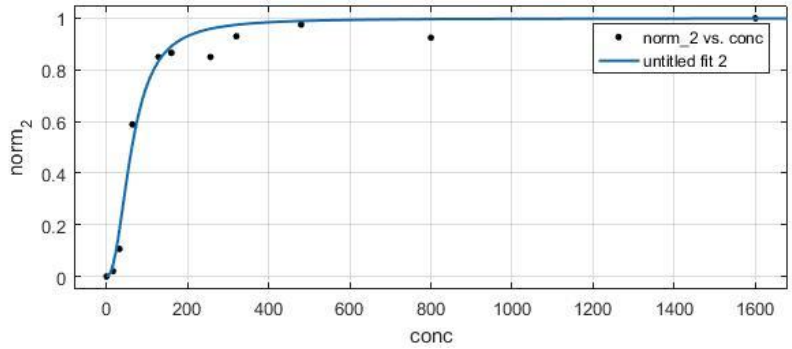

$$y = \frac{1}{1 + (Kd/x)^n}$$

y = % (normalized band intensity)
x = [Ca^{2+}]
K_d = Dissociation constant
n = Hill coefficient

Mm CDH23 EC1+2 was the only protein gel that was able to be quantitatively analyzed with ImageJ and fitted to the equation presented in Fig. 3.g. This construct was added to the trypsin binding assay to serve as a control, as previous experimentation determined the K_d to be 86.8 μM[33]. The K_d's do not match exactly, but they do allow me to believe that the results for EC12+13 and EC12+13^{S1316D} are indicative of the truth.

Construct	K_d (μM)	R^2	n (Hill coefficient)
EC1+2 (37)	62.38	0.9700	2.235
EC1+2 (RT)	33.58	0.9571	1.165

The ambiguity presented in band intensity for Mm CDH23 EC12+13 and EC12+13^{S1316D} did not allow for quantitative analysis, but it can be qualitatively analyzed to an extent. Viewing the SDS-PAGE gels for 37°C, it seems that these two constructs require a higher Ca^{2+} concentration to protect them from trypsin degradation when compared to EC1+2, as band intensity significantly increases towards the 480 μM concentration. Further data is needed to confirm this difference in K_d, and even more specifically, conclude whether or not this difference has any implications for the physiology of the tip link.

Comparing EC1+2 against EC12+13/EC12+13^{S1316D} seems to be more justified than comparing the two constructs of EC12+13. At first glance, it does seem that EC12+13 does require less Ca^{2+} to protect it from trypsin digestion, therefore indicating that it binds Ca^{2+} to a greater extent than the engineered mutant, EC12+13^{S1316D}. Initially planning this experiment, I predicted that this mutant would have an increased binding capacity for Ca^{2+} because technically it is engineered to do so, with the swapping of the WT serine for the conserved aspartate. However, more experimentation is needed to make any conclusions and DSF will also give us an

idea of the binding capacities in the next section. It was my intention to compare Mm CDH23 EC12+13, EC12+13^{S1316D}, and EC12+13^{D1318N}, but the many trials I conducted produced SDS-PAGE gels that were too ambiguous for analysis.

3.6 Results: Differential Scanning Fluorimetry

All data presented for DSF was conducted in triplicate with CDH23 EC12+13, EC12+13^{S1316D}, and EC12+13^{D1318N}. With three independent measurements for one protein, the fluorescence signal was normalized per run to the maximum intensity over the entire range of data (425 readings) from 10°C to 94.8°C to produce a ratio between 0 and 1.

$$0 - 1.0 = \frac{Signal - MIN(1:425)}{MAX(1:425) - MIN(1:425)}$$

Next, the three calculations for each temperature point were averaged and then graphed, where the T_m is given by the point at which the fluorescence signal equals 0.5.

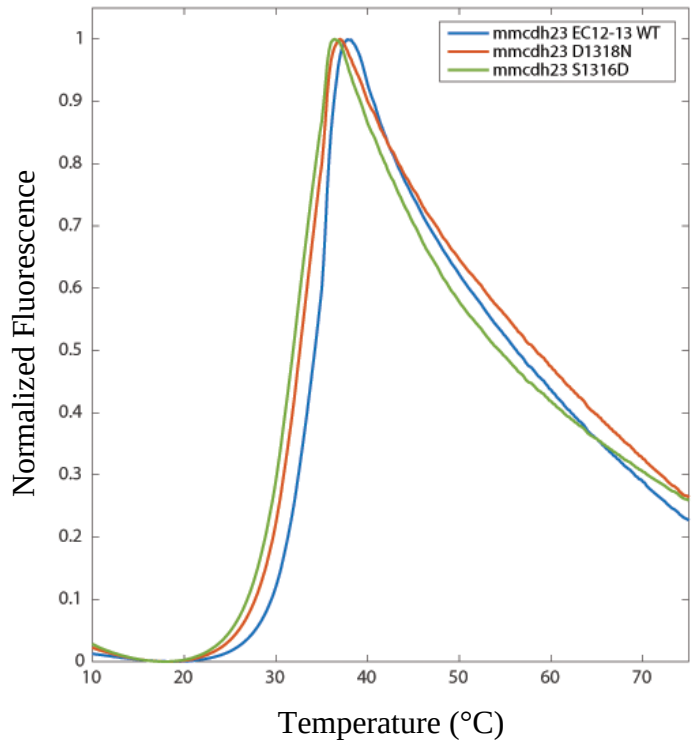

	WT	D1318N	S1316D
Melting Temperature (°C)	34.3	32.6	31.9

Figure 3.g The normalized and averaged DSF spectrum for CDH23 variants performed in triplicate and the experimentally determined melting temperatures.

The data indicates that the melting temperatures for CDH23 EC12+13^{S1316D} and EC12+13^{D1318N} are lower than the WT protein, indicating that the mutations have some effect on the stability of the protein's secondary structure. Additional experiments with DSF will be conducted in the near future to confirm these results.

3.7 Conclusions

It was my hope that this chapter's experimental techniques would show that the non-conserved SXD site afflicted the WT EC12+13 portion of the tip link with a decreased Ca^{2+}-binding affinity and overall decline in stability when compared against the engineered mutant, EC12+13^{S1316D}. Unfortunately, this was not the consensus. One preliminary conclusion from the trypsin assay is that Mm CDH23 EC1+2 maintains a greater Ca^{2+}-binding affinity than both Mm CDH23 EC12+13 and EC12+13^{S1316D}. The other preliminary conclusion from DSF is that the Mm CDH23 EC12+13 construct is more stable than the engineered, EC12+13^{S1316D}, and diseased, EC12+13^{D1318N}, mutant constructs. If the degree of Ca^{2+}-binding is directly correlated with protein stability, then this could indicate that EC12+13 (SXD) does have a higher Ca^{2+}-binding affinity than EC12+13^{S1316D} (DXD) despite the trypsin assay uncertainty. Yet, EC12+13^{D1318N} which is proven to cause deafness creates some distrust in measurements by showing a greater stability than the EC12+13^{S1316D} mutant, despite being close in value.

Contrary to my hypothesis that the decreased stability of the EC12+13 segment of CDH23 does indeed have a physiological role in the overall context of the tip link, this data opens my mind to the possibility that nature knows what it is doing. Is it possible that this variation from aspartate to serine in one-out-of-twenty-seven EC repeats was created to accommodate a unique sequence of amino acids rather than possibly introduce a kink in the tip link like I imagined? I

think it is possible even though I want to believe otherwise, but only time and results will tell its true purpose. In the next section, I look to protein crystallization and X-ray crystallography for answers.

Chapter IV: Protein Crystallization and X-ray Crystallography

Determination of a protein's molecular structure is a significant step towards understanding its function; one that is contingent on a series of experimental techniques succeeding. The stepwise process of refolding the protein, obtaining crystals, collecting a diffraction data set, and diffraction data analysis can take anywhere from months to many years. With nine total wild-type and mutant CDH23 constructs generating roughly one hundred crystal trays over a two year period, it was only recently that I started obtaining protein crystals that were adequate in size to begin X-ray crystallography. In this chapter, I will present crystals of various constructs with and without preliminary diffraction patterns and the methods utilized in my pursuit to someday achieve structural determination.

4.1 Protein Crystallization via Sitting-Drop Vapor Diffusion

In order to make it to this point in the sequence of events, I am able to obtain at minimum 60 µL of well-folded protein; concentrated anywhere from 2-18 mg/mL. Growing protein crystals has become a high-throughput method with the commercialization of crystal screens in which one can test a protein against 96 different buffer conditions in a 96-well plate. The Sotomayor lab has acquired more than ten of these crystallization suites from QIAGEN and Molecular Dimensions that contain different compositions of buffers based off of the type of salt present, the pH of the buffer, and the presence of possible co-factors including various precipitants. A popular method, and the only technique I employed, for the crystallization of macromolecules is sitting drop vapor diffusion. All crystals presented were grown and stored at 4°C.

This method involves the addition of 75 µL of a unique buffer composition to the reservoir buffer, the addition of different ratios of protein:buffer in µL (0.6:0.6, 0.5:1.0, or 1.0:0.5 depending on the concentration and the amount of protein you have available) to the drop support, and the sealing of the tray with pressure sensitive tape (Fig. 4.a). Please note that this process is carried out for each of the 96 wells to test for different buffer compositions and takes only about ten minutes per tray thanks to multi-channel and automated dispensing pipettes. Vapor diffusion exploits the reagent concentration difference between the two separate wells of liquid as they move towards equilibrium, resulting in the diffusion of water from the drop support to the reservoir buffer because it contains a greater reagent concentration. As water leaves the drop support containing our protein of interest, the sample undergoes an increase in relative supersaturation until equilibrium is reached.

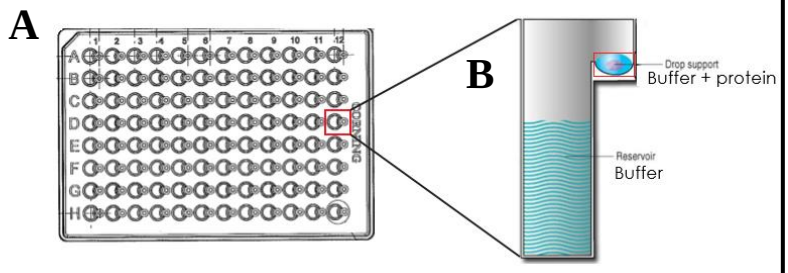

Figure 4.a Setting a crystal tray for sitting drop vapor diffusion **A)** The 96-well plate **B)** A zoomed in view of a single well that effectively separates the "reservoir buffer" from the "drop support" so vapor diffusion can proceed

Successful growth of a crystal does not stem from merely reaching the supersaturation level, but identifying the ideal parameters for inducing nucleation at the lowest degree of supersaturation within the "labile zone". The phase diagram (Fig 4.b A) illustrates just how important this degree of supersaturation is; at high enough levels, the protein becomes an unusable precipitate and if you do not reach supersaturation, the drop containing the soluble protein remains clear and void of crystals. In between these two extremes, the labile zone is desired for nucleation because as the protein concentration gradually decreases, the system will

be driven into the metastable zone of saturation where crystal growth is optimal. Nucleation is the first step in crystallization and it refers to the three-dimensional ordering of an adequate amount of molecules to form a "critical nucleus", or thermodynamically stable aggregate that can provide a surface suitable for further crystal growth. From here, nucleation can proceed to crystal growth if diffusion results in the proper assembly of ordering molecules to the critical nuclei.

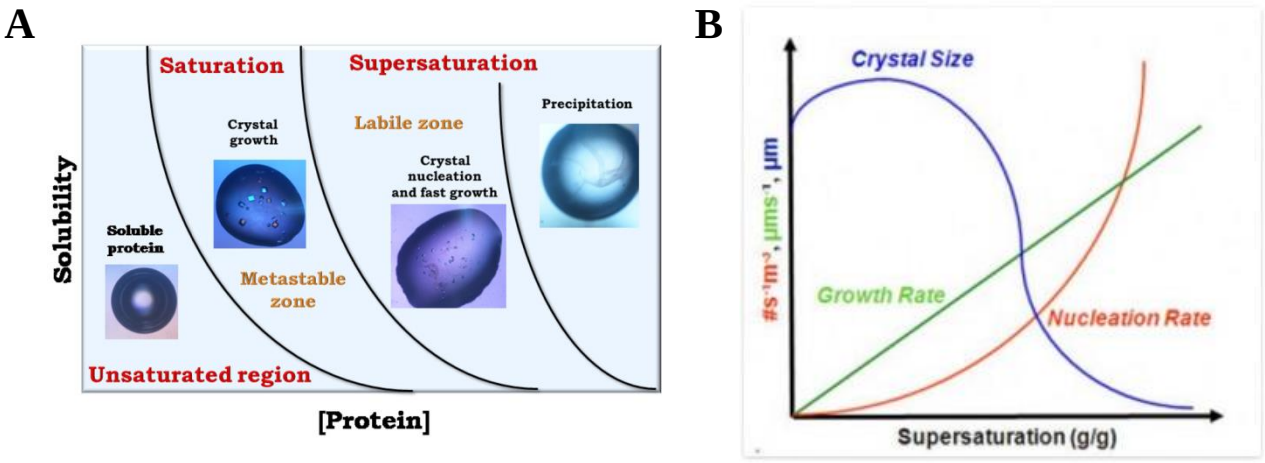

Figure 4.b The degree of supersaturation is critical **A)** The solubility phase diagram for protein crystallization. This diagram illustrates the stable states (liquid, crystalline, precipitate) as a function of two crystallization variables. Adapted from [53] **B)** The relationship for supersaturation vs. crystal size, growth rate, and nucleation rates. A high supersaturation rate results in small crystal growth whereas a low supersaturation rate results in faster and larger crystal growth. Adapted from [54]

Unfortunately, it is not yet possible to identify the ideal conditions to support this process so it becomes a guess, check, and pursue strategy. To guess, thousands of buffer conditions are tested via sitting drop vapor diffusion for each construct. Periodically, the crystal trays are checked for any sign of growth and a plan of action is devised. With a crystal "hit", the conditions that supported growth can be pursued in a number of ways to increase the size and/or

diffraction capabilities of the crystal. This is known as "refining a crystal hit" and various methods such as setting refinement screens, additive screens, and seeding experiments can be conducted.

4.2 Refining Crystallization Conditions for Optimal Crystal Growth

Even though crystal growth is promising to see in the initial screens, these hits are typically used for the identification of crystallization/nucleation conditions that will allow for a more focused crystallization effort. It is important to understand that the size and/or beauty of the crystal does not guarantee a high-resolution diffraction pattern so many crystals of various shapes and forms are often needed. The examples provided were all conducted on Mm CDH23 EC12+13^{D1318N}.

Refinement screens around the buffer that produced the crystal are a smart first choice for expanding the conditions of the initial lead. The initial buffer hit was 0.1 M MES pH 6.5 and 1.5 M $MgCl_2$. The composition table (Fig. 4.c) was made in lab (versus ordering from a company) and sitting drop vapor diffusion with a 96-well plate was conducted in the same way as described above.

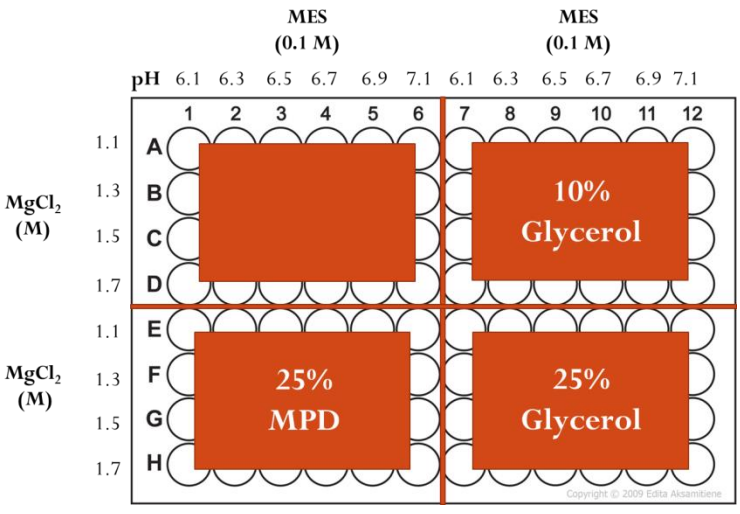

Figure 4.c Designing a refinement screen around a buffer composition that produced a crystal hit. The concentration gradient of $MgCl_2$, the 0.1 M MES pH, and the percentage of cryoprotectant are variables that can alter crystal formation for better or worse.

The initial buffer hit [0.1 M MES pH 6.5, 1.5 M $MgCl_2$] can also be manipulated to create an additive screen. In this method, the concentrations of the initial buffer hit are not altered, but instead are held constant while adding one of 96-unique reagents (multivalent cations, amino acids, dissociating agents, linkers, polyamines, co-factors, etc.) to each well from the Additive Screen HT created by Hampton Research. I added 67.5 µL of the initial buffer hit and 7.5 µL of a single unique reagent from the additive screen to each reservoir buffer well for a total of 75 µL. Next, 0.6 µL of the protein solution ranging from 2-18 mg/mL is added to the drop support and 0.6 µL of the buffer/additive cocktail is transferred from the reservoir buffer to the drop support. Vapor diffusion will then occur normally with the hope of producing different crystals that will diffract to a higher resolution.

The last technique I have tried is known as random microseed matrix screening (rMMS). This method is based off the idea that even though a condition may support nucleation, this same condition may not be optimal for subsequent crystal growth and vice versa[43]. It involves collecting nucleated material from one condition and transferring it to another in the attempt of accessing new and unexplored crystallization space. Proponents of this technique claim that it is a viable method for improving crystal size, number, and quality of existing crystals or crystalline material. First, the seed stock is obtained by selecting several crystallization hits of the same protein and thoroughly crushing the crystals in the drop support with a modified Pasteur pipette (Fig 4.d). After this is accomplished, 50 µL of buffer from the reservoir solution and the crushed nucleation material, verified by viewing the results under a microscope, is added to a 1.5 mL microcentrifuge tube containing a Seed Bead designed by Hampton Research. The suspension is vortexed for 2 minutes, stopping every 30 seconds to cool the tube on ice.

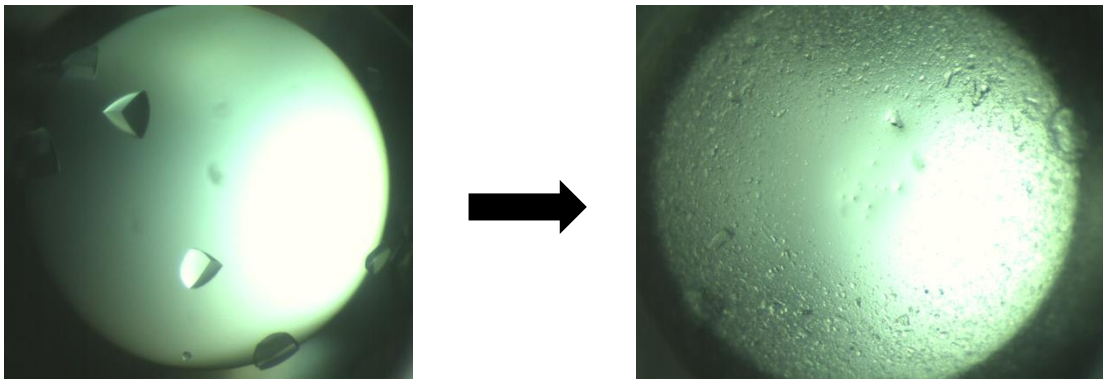

Figure 4.d Before and after crushing crystalline material of Mm CDH23 EC12+13^{D1318N} for a seed stock to be used for rMMS. The tip of a Pasteur pipette was heated with a Bunsen flame, pulled apart at the ends, broken, and plunged repeatedly into the flame to form an ~0.75 mm sphere of glass at the end. This probe was used for crushing the crystals.

At this point in my research, I have gone no further than one round of rMMS with each construct so the seed stock was not diluted[43]. rMMS is typically utilized to test the nucleated protein in entirely different crystallization suites as I had done with Mm CDH23 EC12-14, but for Mm CDH23 EC12+13^{D1318N} I decided to reapply the nucleated protein to the refinement screen that generated the crystals used for seed stock. Each reservoir buffer received 75 µL of buffer (remember that each well is comprised of a different buffer solution) and the drop support got 1 µL of protein solution, 0.5 µL of the seeding solution, and 1 µL that was transferred from reservoir buffer to the drop support. Note that the protein solution is identical to the protein that was harvested for the seed solution, it is well-folded and will, in theory, grow off of the added nucleated material.

4.3 Results: Crystallization Efforts of Various Mm CDH23 Constructs

Structure	CDH23 EC1+2^{D135S}	CDH23 EC12+13^{S1316D}	CDH23 EC12+13^{D1318N}
	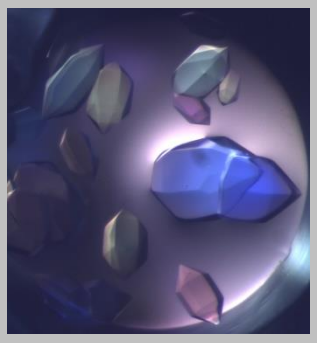	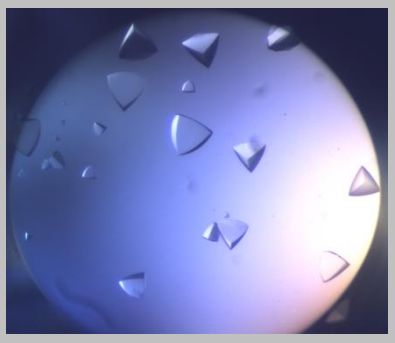	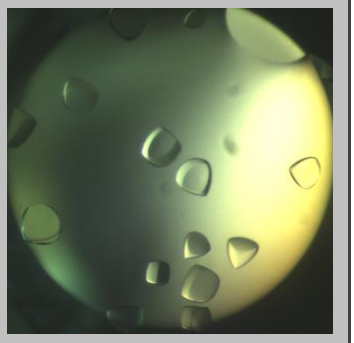
Conditions	0.1 M CaOAc 0.1 M MES pH 6.0 15% PEG 400	1.3 M $MgCl_2$ 0.1 M MES pH 6.3 10% glycerol	1.3 M $MgCl_2$ 0.1 M MES pH 6.5 10% glycerol
Space Group	P6522	N/A	N/A
Resolution	3.07 Å	4.2 Å	5.29 Å

In December of 2015, I sent more than thirty crystals from constructs including Mm CDH23 EC1+2^{D135S}, EC12+13^{S1316D}, EC12+13^{D1318N} and EC12-14^{S1316D} to the Argonne National Laboratory synchrotron. Whereas a complete diffraction data set can take one to three days to complete at the home source, this process is completed in a matter of seconds at this advanced photon source in Illinois by using high-brilliance X-ray beams. Although I am thankful for finally growing crystals after setting fruitless crystal trays during my first two years with the lab, the resolutions for all but EC1+2 are at the upper limit. I am still hopeful that EC12+13^{S1316D} can be solved to provide a rough estimate of the proteins overall shape, but EC12+13^{D1318N} will not be pursued at this resolution. The EC12+13^{S1316D} and EC12+13^{D1318N} crystals shown above are

the result of a refinement screen produced by former lab member Carissa Klanseck around the condition [0.1 M MES pH 6.5, 1.5 M $MgCl_2$]. Looking at the figure above, note that these crystals were grown in very similar conditions with just a small shift in pH despite having two amino acid variations at the Ca^{2+}-binding site.

4.4 Diffraction Data Collection for CDH23 Constructs

In order to collect useful data, the protein crystals must be harvested from the crystallization drop in a process known as "crystal fishing" and mounted on a diffractometer to be bombarded with x-rays. The task begins by isolating a droplet of protein crystals from the drop support onto a coverslip. A gradient of cryoprotectant, a molecule that will cool to cryogenic temperatures without ice formation and damage to the crystal, ranging from low to high concentrations are equilibrated with the crystals to prepare them for the -195.95 °C temperature of liquid nitrogen. Typical cryoprotectants include compounds like PEG, sucrose, or glycerol.

Figure 4.e A mounted cryogenic loop with a crystal ready for X-ray crystallography to commence. Notice the mother liquor stuck within the loop and the lack of ice formation due to cryoprotection. Adopted from [55]

Looking through the microscope, one uses a cryogenic loop (Hampton Research) ranging from 0.05, 0.1, 0.2, or 0.3 mm dependent on the size of the crystal to catch and pick up the selected target crystal. Once in the loop and surrounded by mother liquor, the single crystal is immediately flash-cooled in liquid nitrogen and stored for future data collection on an X-ray beamline. Cryoprotection is very important for the freezing of the crystal and for data collection,

as crystals can potentially crack if subjected to such an extreme temperature difference and suffer severe damage from high X-ray radiation if not protected.

Diffraction data was remotely collected on the 24 ID-E of the Advance Photon Source (APS) at Argonne National Laboratory. This fixed energy beamline is optimized to address challenging cases in macromolecular crystallography such as poorly diffracting crystals and microcrystals by providing extremely stable and intense x-ray beams with beam sizes ranging from 5 to 70 microns. The data was collected with the ADSC Q315 3X3 CCD/AMPTEK XR-100SDD detectors. Most of the crystal screening, a test to determine whether crystals are protein or salt, was conducted at the home source with a Rigaku MicroMax 003 and Pilatus 200k detector.

4.5 From Diffraction Pattern to Atomic Model: Data Analysis of CDH23 EC1+2^{D135S}

The crystal has now been illuminated with an X-ray source to provide a plethora of information, despite appearing as a random assortment of black dots arrayed on the computer screen (Fig 4.f). The first task involves indexing, integrating, and then scaling the data set with HKL2000 (Otwinowsk and Minor, 1997). Indexing involves measuring the intensities of the spots for one diffraction image and a preliminary fitting to one of fourteen Bravais lattices, providing information such as unit cell parameters and the orientation of the crystal.

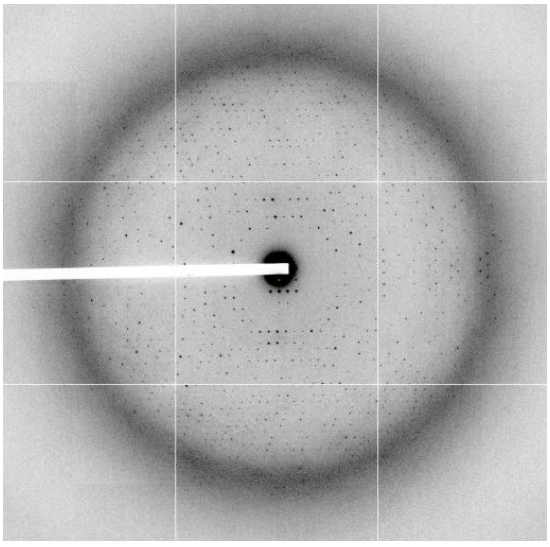

Figure 4.f The diffraction pattern for EC1+2^{D135S}. This symmetrical pattern belongs to the P6522 space group

Once this information is optimized, integration can be performed to fit the rest of the diffraction images to the same parameters. In the final step of scaling and merging, the software attempts to put all observations on a common scale. With this completed, it was determined that my EC1+2^{D135S} crystal diffracted to 3.068 Å and was categorized by the P6522 space group.

All of the information needed to solve the structure is now available, except for the phase information. An integrated suite of programs for macromolecular X-ray crystallography called ccp4i was utilized to elucidate this information. First, the output file must be converted to an mtz file with the program "Scalepack2mtz". This software also analyzes the data for a common problem facing structural determination where inter-nuclei growth of two crystals is exhibited, a scenario known as twinning. Fortunately, twinning was not evident in my data set so I continued and calculated the matthews coefficient with the program "Matthews_coef". This software predicts the number of molecules in the asymmetric unit and it was determined to be only one for the EC1+2^{D135S} crystal. This is the best possible result, as more molecules in the asymmetric unit require more work in the refinement, which will be further touched upon. Finally, the phase issue is best addressed with molecular replacement in this situation because it provides starting phases from a correctly positioned structurally similar model and, if sufficient, can be used to obtain an interpretable electron density map. This

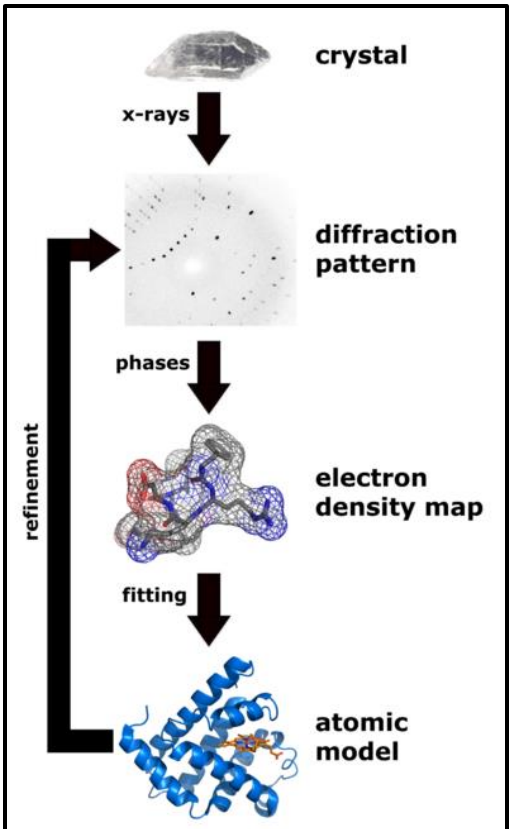

Figure 4.g The sequence of events leading to obtaining an atomic model for the protein of interest. I am currently working on electron density reconstruction. Image adopted from [56]

was exactly the case and “Phaser MR” was able to fit the phase information by searching with the individual, truncated structures of EC1 and EC2, PDB code 2WHV, that were previously determined by Marcos Sotomayor[33]. Currently, I am using real- and reciprocal-space refinement to fit the structure generated from molecular replacement with Mm CDH23 EC1+2 to the experimentally obtained electron density map of CDH23 EC1+2^{D135S}.

Data collection	**Mm CDH23 EC1+2**
Space group	P6522
Unit cell parameters	
a, b, c (Å)	132.14, 132.14, 136.69
$\alpha\beta\gamma$ (°)	90, 90, 120
Molecules per asymmetric unit	1
Beam source	APS-24-ID-E
Wavelength (Å)	0.9792
Resolution limit (Å)	3.07
Unique reflections	13693
Completeness (%)	99.63 (98.78)
Redundancy	5.8 (5.7)
I / $\sigma(I)$	22.63 (2.00)
R_{merge}	0.102 (1.24)
R_{meas}	0.107 (1.30)
R_{pim}	0.032 (0.39)
$CC_{1/2}$	(0.68)
CC^*	(0.90)
Refinement	
Resolution range (Å)	114.32 – 3.07 (3.148 – 3.068)
R_{work} (%)	22.2 (33.2)
R_{free} (%)	25.1 (52.5)
Residues (atoms)	208
Ligand/ion	4
Water molecules	N/A
Rms deviations	
Bond lengths (Å)	0.0152
Bond angles (□)	1.8943
B-factor average	93.009
Ramachandran Plot Region (PROCHECK)	
Most favored (%)	80.0
Additionally allowed (%)	17.2
Generously allowed (%)	2.8
Disallowed (%)	0.0
PDB ID code	**Not completed**

Figure 4.h Data collection statistics of EC1+2^{D135S}

4.6 Conclusions

Before this semester, I was trying to figure out why crystals were not growing for my constructs. Now that I solved that mystery and produced beautiful crystals that do not diffract well, I am met with the new challenge of making them "better". This does not mean a bigger or more geometrically shaped crystal, this means any method that will produce or alter the crystals so that they diffract to a sufficient resolution for structural determination. This can be accomplished in two ways: growing new crystals or affecting the properties of those already in my crystal trays.

I illustrated the use of refinement screens, additive screens, and seeding methods in this chapter, but different techniques will also be implemented. Cryoprotection is a crucial aspect of preparing protein crystals for X-ray diffraction[44], yet I have neglected the influence these compounds may have on the potential diffraction. Every crystal thus far has been protected with glycerol and I need to try others such as MPD, PEG 400, ethylene glycol, etc. I have focused much of my time on finding the ideal buffer conditions to grow crystals and maybe the cryoprotectant needs to be held to this same standard. Additionally, I will try shooting non-frozen crystals, soaking the crystals in conditions of higher precipitant to shrink the cell, and annealing methods in which temperature variations from cryogenic to room temperature alters the crystalline properties. With this, I am hopeful that I will overcome the setback of poor diffracting crystals.

Finally, I would like to address why the Mm CDH23 EC12+13^{S1316D} and Mm CDH23 EC12+13^{D1318N} proteins produce very similar looking crystals whereas Mm CDH23 EC12+13 has only been crystallized once; to give a very small, weakly diffracting crystal at that. I do not have an answer, but I would like to think that the protein stability plays an important part in

crystallization. Is it possible that both the engineered and diseased mutant constructs crystallize better than the wild-type construct because of a decreased protein stability? It is a possibility and one that I hope to have an answer for within the coming months.

Chapter V: Future Directions

The essence of hearing revolves around understanding every biochemical and physiological aspect of the tip link. The Sotomayor lab is working diligently to elucidate the entire structure of this molecular machinery to better understand function in its entirety. My purpose for working with Mm CDH23 is to explore the variation from aspartate to serine located at the SXD site between EC12 and 13. Why would mother nature change a conserved Ca^{2+}-binding residue in only one out of twenty seven instances without a purpose? Tackling the problem from two different approaches, structural determination paired with biochemical methods to measure Ca^{2+}-binding affinities was utilized to obtain preliminary results detailed in their respective chapters. With all experimental evidence pointing at the importance of Ca^{2+}, I am still hopeful that I will find an abnormal binding site that serves of crucial importance to the tip link yet to be determined, but the trypsin assays and DSF results comparing Mm CDH23 EC12+13, EC12+13^{S1316D}, and EC12+13^{D1318N} show zero supporting evidence for this.

With only four months left in the lab, I am on a mission to obtain a high resolution diffraction pattern of Mm CDH23 EC12+13^{S1316D} and/or Mm CDH23 EC12+13^{D1318N}. There are more than enough crystals ready to be screened and I maintain the faith that one of them will be it. The opportunity to be the first person to decipher the structure surrounding the Ca^{2+}-binding site of interest and contribute to great research would be the highlight of my college career.

A

Additive (B5)	Additive (C8)	Additive (H5)
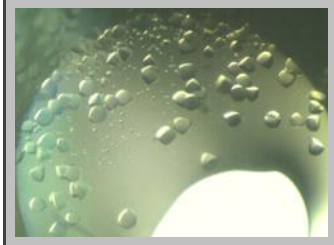		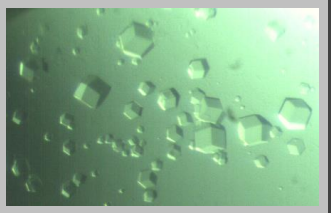
0.1 M MES pH 6.3 1.3 M $MgCl_2$ 10% glycerol 1.0 M LiCl	0.1 M MES pH 6.3 1.3 M $MgCl_2$ 10% glycerol 30% w/v 1,6-Diaminohexane	0.1M MES pH 6.3 1.3 M $MgCl_2$ 10% glycerol 40% v/v Formamide

Figure 5.a Protein crystals yet to be screened **A)** An additive screen produced the following crystals for Mm CDH23 EC12+13^{S1316D}. The crystal grown in B5 is indicative of many more crystals not pictured, but the C8 and H5 crystals have a unique cube shape that is not seen in other buffer conditions **B)** An additive screen and random microseed matrix screening produced the following crystals for Mm CDH23 EC12+13^{D1318N} plus many more not pictured. The C4 and G2 crystals are very similar in shape to crystals that have been determined to not diffract well. However, this has no bearing on how well they will diffract, it must be determined experimentally. The C2 and C6 crystals from a previous refinement screen I created are the first crystals I have grown from seeding so I am excited to screen them as they look different in shape from the typical crystals I grow.

B

Additive (C4)	Additive (G2)	Seeding (Ref 05 – C2)	Seeding (Ref 05 – C6)
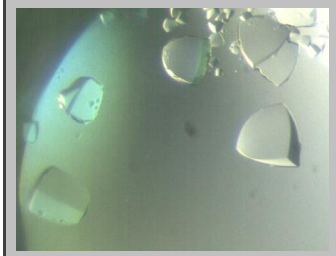		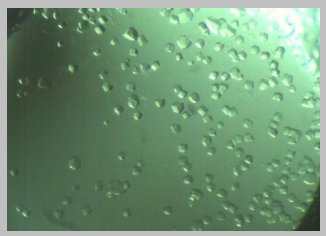	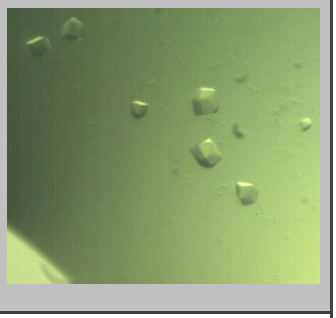
0.1 M MES pH 6.5 1.3 M $MgCl_2$ 10% glycerol 30% v/v Dimethyl Sulfoxide	0.1 M MES pH 6.5 1.3 M $MgCl_2$ 10% glycerol 30% w/v 1,6-Hexanediol	0.1 M MES pH 6.3 1.5 M $MgCl_2$	0.1 M MES pH 7.1 1.5 M $MgCl_2$

Biochemistry Undergrad Spotlight Questionnaire:

Thank you for participating in the Biochemistry Undergrad Spotlight! We will be featuring a new Undergraduate student each month in order to highlight their academic accomplishments and connect with other current and future Biochemistry students. Please fill out the questionnaire to the best of your ability and do not hesitate to ask if you have questions or comments.

1. What is your academic standing, major, and favorite class taken so far at OSU?

   I am a 4th year biochemistry/pre-med student and my favorite class has been Biochemistry 5614, if not the entire biochemistry series. To put the science foundation gained from the biology and general/organic chemistry courses into the context of life was fascinating, especially the highly complex and integrative metabolic processes of our bodies.

2. What is your favorite aspect of working in the Biochemistry Labs?

   It is an awesome experience to join a lab with limited knowledge, get trained to understand the theory and methodology behind your work, and then become more and more independent over time as you develop your own research project. I never thought that as an undergraduate student, I would have an opportunity to contribute new knowledge that could shape the scientific community.

   With two years in *The Sotomayor Research Group*, I have had a wonderful experience in undergraduate research because of the people that surround me. Working with those that have different interests, levels of educational attainment, and backgrounds to solve a common goal not only motivates, but makes you realize what it takes to be successful. The mentorship that comes with research is indispensable.

3. What is the main focus of the research in your lab and what impact do you think it will make?

   As a member of *The Sotomayor Research Group*, I am studying a portion of a protein complex known as the tip link, a core component of vertebrate hearing. From protein biochemistry to X-ray crystallography, I get to utilize a wide range of techniques with the goal of elucidating the molecular mechanisms underlying normal hearing and deafness. Ultimately, by understanding the mechanisms at play, our lab will be able to manipulate the system and contribute to curing some forms of deafness, whether genetic or noise-induced.

   Check us out: https://research.cbc.osu.edu/sotomayor.8/

4. How would you encourage prospective students to engage with the Biochemistry Department?

   If you are a biochemistry student, I would strongly recommend enrolling in Biochemistry 2900H, a course offered in the Autumn semester that allows you to listen to various professors in the department and join a lab based off of your interests (if a spot is available). Equally effective, do not hesitate to contact a professor expressing your interest in their lab; the worst they can say is “no thank you”. Most importantly, professors are people to that are generally very friendly, easy to talk to, and excited that you have taken interest in their work. Also, research forums are a great way to interact with your peers and identify subjects that may be of interest to you.

5. What advice would you give to future students studying Biochemistry?
   Do NOT let your current knowledge or academic standing hold you back from partaking in research. From personal experience, I arrived at Ohio State without a strong foundation in science; illustrated by the fact that proteins were foreign to me until my first biology course. Honestly, I was intimidated by not only the complexity of research topics, but by the thought of working with other undergrads, graduate students, and post-docs that are brilliant. Yet, I caught on and you will as well; it is amazing how fast you learn when you can interact with science outside of a textbook.

   Based off of my experience in and around the research community at The Ohio State University, I would advise any future biochemistry student to make it a priority to partake in research; whether you want to get a PhD, go to professional school, or join the workforce right out of college. And do not feel constrained to biochemistry research, explore the many options available and pick a group that suits your interests whether the subject is interpretative dance, the impact of music in developing nations, or studying extended care for piglets. The options are endless and the impact on your education tremendous. Best of luck!

1. Manley GA, Clack JA. An outline of the evolution of vertebrate hearing organs. In: *Evolution of the Vertebrate Auditory System*. Vol 22. New York, NY: Springer New York; 2004:1-26. doi:10.1007/978-1-4419-8957-4_1.
2. Fay RR, Popper AN. Evolution of hearing in vertebrates: The inner ears and processing. *Hear Res*. 2000;149(1-2):1-10. doi:10.1016/S0378-5955(00)00168-4.
3. Kandel ER, Schwartz JH, Jessell TM. *Principles of Neural Science*. Vol 3.; 2013. doi:10.1036/0838577016.
4. Smith R, Hildebrand, Van Camp G. Deafness and Hereditary Hearing Loss Overview. *GeneReviews*. 2010;6:1-13. doi:NBK1434 [bookaccession].
5. Types of Hearing Loss. http://www.asha.org/public/hearing/Types-of-Hearing-Loss/. Accessed March 9, 2016.
6. WHO | Deafness and hearing loss. http://www.who.int/mediacentre/factsheets/fs300/en/. Accessed February 20, 2016.
7. Jacobson BD. 2.972 How The Human Ear Works. http://web.mit.edu/2.972/www/reports/ear/ear.html. Accessed March 9, 2016.
8. Heffner RS, Heffner HE. Evolution of Sound Localization in Mammals. In: Webster DB, Popper AN, Fay RR, eds. *The Evolutionary Biology of Hearing*. New York, NY: Springer New York; 1992:691-715. doi:10.1007/978-1-4612-2784-7.
9. The Middle Ear. http://www.csun.edu/~vcoao0el/webct/de361s81_folder/tsld002.html. Accessed March 9, 2016.
10. Dancer A, Rebillard G. Middle Ear | Cochlea. http://www.cochlea.eu/en/ear/middle-ear. Accessed March 9, 2016.
11. Gray L. Auditory System: Structure and Function (Section 2, Chapter 12). In:

Neuroanatomy Online. http://neuroscience.uth.tmc.edu/s2/chapter12.html. Accessed March 8, 2016.

12. Manley GGA, Popper ANA, Fay RRR. *Evolution of the Vertebrate Auditory System*.; 2004. doi:10.1007/978-1-4419-8957-4.
13. Local PM. Prestin is required for electromotility of the outer hair cell and for the cochlear amplifier. *Nature*. 2002;419(September):300-304. doi:10.1038/nature01001.1.
14. Salt AN, Inamura N, Thalmann R, Vora A. Calcium gradients in inner ear endolymph. *Am J Otolaryngol Neck Med Surg*. 1989;10(6):371-375. doi:10.1016/0196-0709(89)90030-6.
15. Axelrod JD. Basal bodies, kinocilia and planar cell polarity. *Nat Genet*. 2008;40(1):10-11. doi:10.1038/ng0108-10.
16. Alberti PW. The Anatomy and Physiology of the Ear and Hearing. In: *Occupational Exposure to Noise: Evaluation, Prevention and Control*. ; 1995:53-62. http://www.who.int/occupational_health/publications/noise2.pdf. Accessed March 8, 2016.
17. Angst BD, Marcozzi C, Magee AI. The cadherin superfamily: diversity in form and function. *J Cell Sci*. 2001;114(4):629-641.
18. Brasch J, Harrison OJ, Honig B, Shapiro L. Thinking outside the cell: How cadherins drive adhesion. *Trends Cell Biol*. 2012;22(6):299-310. doi:10.1016/j.tcb.2012.03.004.
19. Elledge HM, Kazmierczak P, Clark P, et al. Structure of the N terminus of cadherin 23 reveals a new adhesion mechanism for a subset of cadherin superfamily members. *Proc Natl Acad Sci*. 2010;107(23):10708-10712. doi:10.1073/pnas.1006284107.
20. Ahmed ZM, Goodyear RJ, Riazuddin S, et al. The tip-link antigen, a protein associated with the transduction complex of sensory hair cells, is protocadherin-15. *J Neurosci*.

2006;26(26):7022-7034. doi:10.1523/JNEUROSCI.1163-06.2006.

21. Kazmierczak P, Sakaguchi H, Tokita J, et al. Cadherin 23 and protocadherin 15 interact to form tip-link filaments in sensory hair cells. *Nature*. 2007;449(7158):87-91. doi:10.1038/nature06091.

22. Alagramam KN, Murcia CL, Kwon HY, Pawlowski KS, Wright CG, Woychik RP. The mouse Ames waltzer hearing-loss mutant is caused by mutation of Pcdh15, a novel protocadherin gene. *Nat Genet*. 2001;27(1):99-102. doi:10.1038/83837.

23. Di Palma F, Pellegrino R, Noben-Trauth K. Genomic structure, alternative splice forms and normal and mutant alleles of cadherin 23 (Cdh23). *Gene*. 2001;281(1-2):31-41. doi:10.1016/S0378-1119(01)00761-2.

24. Pickles JO, Comis SD, Osborne MP. Cross-links between stereocilia in the guinea pig organ of Corti, and their possible relation to sensory transduction. *Hear Res*. 1984;15(2):103-112. http://eutils.ncbi.nlm.nih.gov/entrez/eutils/elink.fcgi?dbfrom=pubmed&id=6436216&retmode=ref&cmd=prlinks.

25. Assad JA, Shepherd GM, Corey DP. Tip-link integrity and mechanical transduction in vertebrate hair cells. *Neuron*. 1991;7(6):985-994. http://eutils.ncbi.nlm.nih.gov/entrez/eutils/elink.fcgi?dbfrom=pubmed&id=1764247&retmode=ref&cmd=prlinks.

26. Siemens J, Lillo C, Dumont RA, et al. Cadherin 23 is a component of the tip link in hair-cell stereocilia. *Nature*. 2004;428(6986):950-955. doi:10.1038/nature02483.

27. Söllner C, Rauch G-J, Siemens J, et al. Mutations in cadherin 23 affect tip links in zebrafish sensory hair cells. *Nature*. 2004;428(6986):955-959.

http://eutils.ncbi.nlm.nih.gov/entrez/eutils/elink.fcgi?dbfrom=pubmed&id=15057246&retmode=ref&cmd=prlinks.

28. Sotomayor M, Weihofen WA, Gaudet R, Corey DP. Structure of a force-conveying cadherin bond essential for inner-ear mechanotransduction. *Nature*. 2012;492(7427):128-132. doi:10.1038/nature11590.

29. Lelli A, Kazmierczak P, Kawashima Y, Müller U, Holt JR. Development and regeneration of sensory transduction in auditory hair cells requires functional interaction between cadherin-23 and protocadherin-15. *J Neurosci*. 2010;30(34):11259-11269. doi:10.1523/JNEUROSCI.1949-10.2010.

30. Pickles JO. *An Introduction to the Physiology of Hearing*. BRILL; 2012. https://books.google.com/books?id=mMTFWiLLw-cC&pgis=1. Accessed March 15, 2016.

31. Cheung ELM, Corey DP. Ca2+ changes the force sensitivity of the hair-cell transduction channel. *Biophys J*. 2006;90(1):124-139. doi:10.1529/biophysj.105.061226.

32. Howard J, Hudspeth AJ. Compliance of the hair bundle associated with gating of mechanoelectrical transduction channels in the bullfrog's saccular hair cell. *Neuron*. 1988;1(3):189-199. http://eutils.ncbi.nlm.nih.gov/entrez/eutils/elink.fcgi?dbfrom=pubmed&id=2483095&retmode=ref&cmd=prlinks.

33. Sotomayor M, Weihofen WA, Gaudet R, Corey DP. Structural determinants of cadherin-23 function in hearing and deafness. *Neuron*. 2010;66(1):85-100. doi:10.1016/j.neuron.2010.03.028.

34. Cailliez F, Lavery R. Cadherin mechanics and complexation: the importance of calcium

binding. *Biophys J*. 2005;89(6):3895-3903. doi:10.1529/biophysj.105.067322.

35. Pokutta S, Herrenknecht K, Kemler R, Engel J. Conformational changes of the recombinant extracellular domain of E-cadherin upon calcium binding. *Eur J Biochem*. 1994;223(3):1019-1026. doi:10.1111/j.1432-1033.1994.tb19080.x.

36. Hladek G. Deaf Culture | The Institute for Applied & Professional Ethics. https://www.ohio.edu/ethics/tag/deaf-culture/index.html. Accessed March 9, 2016.

37. Jones M. Deafness as Culture: A Psychosocial Perspective. *Disabil Stud Q*. 2002;22(2). http://dsq-sds.org/article/view/344. Accessed March 9, 2016.

38. Sliwinska-Kowalska M, Davis A. Noise-induced hearing loss. *Noise Health*. 2012;14(61):274-280. doi:10.4103/1463-1741.104893.

39. Schwander M, Xiong W, Tokita J, et al. A mouse model for nonsyndromic deafness (DFNB12) links hearing loss to defects in tip links of mechanosensory hair cells. *Proc Natl Acad Sci U S A*. 2009;106(13):5252-5257. doi:10.1073/pnas.0900691106.

40. NIH MBI Laboratory for Structural Genomics and Proteomics. http://nihserver.mbi.ucla.edu/RACC/. Accessed March 17, 2016.

41. Palmer I, Wingfield PT. Preparation and extraction of insoluble (Inclusion-body) proteins from Escherichia coli. *Curr Protoc Protein Sci*. 2012;1(SUPPL.70). doi:10.1002/0471140864.ps0603s70.

42. Ericsson UB, Hallberg BM, DeTitta GT, Dekker N, Nordlund P. Thermofluor-based high-throughput stability optimization of proteins for structural studies. *Anal Biochem*. 2006;357(2):289-298. doi:10.1016/j.ab.2006.07.027.

43. Till M, Robson A, Byrne MJ, et al. Improving the success rate of protein crystallization by random microseed matrix screening. *J Vis Exp*. 2013;(78):1-6. doi:10.3791/50548.

44. McFerrin MB, Snell EH. The development and application of a method to quantify the quality of cryoprotectant solutions using standard area-detector X-ray images. *J Appl Cryst*. 2002;35(1996):538-545.

45. Figure 44-4. https://www.dartmouth.edu/~humananatomy/figures/chapter_44/44-4.HTM. Accessed March 15, 2016.

46. Purves D, Augustine GJ, Fitzpatrick D. *Neuroscience*.; 2004. doi:978-0878937257.

47. Hudspeth a J. The cellular basis of hearing: the biophysics of hair cells. *Science*. 1985;230(4727):745-752. doi:10.1126/science.2414845.

48. Furness DN, Hackney CM. High-resolution scanning-electron microscopy of stereocilia using the osmium-thiocarbohydrazide coating technique. *Hear Res*. 1986;21(3):243-249. doi:10.1016/0378-5955(86)90222-4.

49. Kachar B, Parakkal M, Kurc M, Zhao Y, Gillespie PG. High-resolution structure of hair-cell tip links. *Proc Natl Acad Sci U S A*. 2000;97(24):13336-13341. doi:10.1073/pnas.97.24.13336.

50. Sotomayor M, Gaudet R, Corey DP. Sorting out a promiscuous superfamily: towards cadherin connectomics. *Trends Cell Biol*. 2014. doi:10.1016/j.tcb.2014.03.007.

51. Humphrey W, Dalke A, Schulten K. VMD: visual molecular dynamics. *J Mol Graph*. 1996;14(1):33-38. http://eutils.ncbi.nlm.nih.gov/entrez/eutils/elink.fcgi?dbfrom=pubmed&id=8744570&retmode=ref&cmd=prlinks.

52. GE Healthcare Life Sciences. Size Exclusion Chromatography. In: *Handbooks*. ; :139. http://www.gelifesciences.com/webapp/wcs/stores/servlet/catalog/en/GELifeSciences-us/service-and-support/handbooks/. Accessed March 21, 2016.

53. Krauss IR, Merlino A, Vergara A, Sica F. An overview of biological macromolecule crystallization. *Int J Mol Sci*. 2013;14(6):11643-11691. doi:10.3390/ijms140611643.

54. O'Grady D. Supersaturation: Driving Force For Crystal Nucleation & Growth | Chemical Research, Development And Scale-up. http://blog.autochem.mt.com/2011/03/supersaturation-driving-force-for-crystal-nucleation-growth/. Accessed April 3, 2016.

55. Mac Sweeney A, D'Arcy A. A simple and rapid method for mounting protein crystals at room temperature. *J Appl Crystallogr*. 2003;36(1):165-166. doi:10.1107/S0021889802019623.

56. Splettstoesser T. SciStyle. http://www.scistyle.com/. Accessed April 6, 2016.